

NASA Technical Memorandum 85662

NASA-TM-85662 19840007049

Flow Improvements in the Circuit of the Langley 4- by 7-Meter Tunnel

Zachary T. Applin

DECEMBER 1983



25th Anniversary
1958-1983

NASA

ERRATA

NASA Technical Memorandum 85662

FLOW IMPROVEMENTS IN THE CIRCUIT OF THE
LANGLEY 4- BY 7-METER TUNNEL

By Zachary T. Applin

December 1983

In figures 6(a) and (c), the labels at the top of the plots should read "Bottom" and "Top" instead of "Inner wall" and "Outer wall," respectively. The abscissa label in each plot should read "z/h" instead of "y/w."

ISSUE DATE: December 1983



NASA Technical Memorandum 85662

Flow Improvements in the Circuit of the Langley 4- by 7-Meter Tunnel

Zachary T. Applin
*Langley Research Center
Hampton, Virginia*



**Scientific and Technical
Information Branch**

1983

SUMMARY

In order to identify the most promising means for improving the flow in the circuit of the Langley 4- by 7-Meter Tunnel, a series of investigations were conducted to determine the mean flow characteristics in the wind-tunnel circuit. Detailed surveys of the mean velocity profiles were measured in both the horizontal and vertical planes of symmetry at specific stations throughout the tunnel circuit. These data were obtained at test-section dynamic pressures of 1.53, 2.78, and 4.79 kPa (32, 58, and 100 psf, respectively) for tunnel operation in both the closed and open test-section configurations.

In the base-line tunnel-flow surveys, the flow patterns near the end of the test section indicate a uniform mean velocity distribution spanning essentially the entire width of the test section. Downstream of the test section, the flow patterns in the three diffusers upstream of the drive fan indicate a flow that is skewed toward the outer wall. This flow results in low velocities along the inner walls, flow separation midway through the third diffuser (just upstream of the drive fan), and very unsymmetrical flow entering the drive fan. In the large fourth diffuser downstream of the drive fan, the unsymmetrical flow exiting the drive fan leads to complete flow separation from the outer wall and development of a large zone of reversed flow. In order to correct these unsymmetrical flow patterns, a tunnel modification, consisting of a set of trailing-edge flaps attached to the five flow-control vanes located just downstream of the first corner, was designed to deflect the flow more toward the inner wall. These flaps were very successful in making the tunnel flow more symmetrical and completely eliminated the regions of separation in the diffusers upstream and downstream of the drive fan. This modification provides a much improved base-line tunnel flow in preparation for the scheduled installation in 1984 of four screens and one honeycomb in the entrance to the contraction.

INTRODUCTION

The need for subsonic and transonic wind tunnels with excellent flow quality has been recognized, and progress is being made in developing and improving such tunnels. (See refs. 1 to 4.) The improvement of the tunnel-flow quality is an important part of an ongoing project to improve the efficiency and productivity of the Langley 4- by 7-Meter Tunnel. A significant step in this direction will be accomplished with a scheduled major facility modification to be completed in 1984. In preparation for this improvement project, several factors led to the investigation of the flow characteristics throughout the tunnel circuit. Based on unpublished calibration data, the mean velocity profiles in the test section are very uniform and the tunnel is currently very good for conventional model force and pressure testing; however, the airstream through the test section is characterized by a somewhat meandering and random fluctuation of the flow.

Previous unpublished tuft studies indicated extensive regions of separated flow in the large diffuser downstream of the drive fan. This separated-flow region was a concern because the eddies that are produced can feed into the airstream, travel around the circuit, and be contracted into the test section. By the use of long data-sampling periods, these unsteady-flow effects can be averaged out of most

aerodynamic force and pressure measurements at the expense of tunnel power. However, these problems become more critical for detailed dynamic flow-field measurements around small-scale models. (See ref. 2.) In particular, the separation and asymmetry of the airstream has presented a significant problem for laser-velocimeter (LV) measurements. The artificial seeding of the flow required for LV measurements in this facility is achieved through the use of a particle generator placed at a specific location in the settling chamber. This location is varied to produce a stream of seeding particles at desired LV measurement locations in the test section. Because of the existing flow separation and asymmetry, this seeding process has required an extensive search for the particle-generator location necessary to produce seeding particles at the desired location in the test section.

The purpose of this investigation was to document the mean flow characteristics throughout the base-line tunnel circuit and determine the appropriate means of improving the flow. Mean velocity profiles have been measured in both horizontal and vertical planes of symmetry at various stations throughout the tunnel circuit. The data presented in this report were obtained soon after the dense debris-catching screen at the second corner, which covered the entire cross-sectional area, was replaced by a less-dense screen which covered only the lower third of the cross-sectional area. The dense debris-catching screen was replaced because of its extremely high resistance, which increased the power losses in the tunnel circuit excessively and limited the test-section maximum velocity. The removal of this dense screen resulted in a 33-percent reduction in the tunnel drive power at a test-section dynamic pressure of 2.78 kPa (58 psf).

This report documents the results to date in preparation for future tunnel modifications which will include the scheduled installation in 1984 of four screens and one honeycomb in the entrance to the contraction.

SYMBOLS

The values presented in this report are given in the International System of Units (SI) with the equivalent values given parenthetically in the U.S. Customary Units. All measurements and calculations were made in the U.S. Customary Units.

h tunnel-circuit height at indicated station, m (ft)

q dynamic pressure, kPa (psf)

u local measured flow velocity, m/sec (ft/sec)

w tunnel-circuit width at indicated station, m (ft)

y lateral distance from inner tunnel wall, m (ft)

z vertical distance above tunnel floor, m (ft)

Subscripts:

max maximum

TS test section

Abbreviations:

CTS	closed test section
FCV	flow-control vane
LV	laser velocimeter
OTS	open test section

TUNNEL DESCRIPTION

The Langley 4- by 7-Meter Tunnel (see fig. 1) is a closed-circuit, single-return, atmospheric wind tunnel. Figure 2 shows a plan-view sketch of the tunnel circuit with the velocity-traverse measurement stations indicated. These traverse stations were chosen to coincide with a previous set of similar velocity-profile measurements (see ref. 5) that were obtained before the removal of the dense debris-catching screen on the second corner. The test section is 4.42 m (14.5 ft) high by 6.63 m (21.75 ft) wide by 15.2 m (50.0 ft) long. The test-section speed is variable from 0 to 103 m/sec (0 to 200 knots). The test section can be operated in a variety of configurations - closed, slotted, partially open, and open. The open test-section configuration is open only on three sides. The walls and ceiling are raised, but the floor remains in place. The primary use of the tunnel has been for low-speed, steady-state aerodynamics. A limited use of the tunnel has been made for acoustic and flow-field testing.

EQUIPMENT DESCRIPTION

Velocity profiles were measured by using a miniature flow-direction and air-speed sensor described in reference 6. A typical installation for horizontal-velocity-profile measurements is shown in figure 3, which shows the sensor mounted at station 2 for the open test-section configuration. The sensor measures the oncoming flow speed by using a small-propeller anemometer. A small 3.18-cm-diameter (1.25-in.) propeller was used at stations 1, 2, and 20. A larger 5.08-cm-diameter (2.00-in.) propeller was used at all other stations. The overall accuracy of the flow-speed measurement is ± 1 m/sec (± 3.281 ft/sec). Data were obtained at the rate of 50 samples per second for 5 sec.

A typical calibration of both the low- and high-speed sensors is presented in figures 4(a) and (b), respectively. This sensor normally has the capability of measuring the pitch and yaw angles of the oncoming flow. However, because of the method of mounting and traversing the sensor, this capability was frequently lost as a result of instrumentation failure. The limited angular measurements that were obtained were inconclusive because of large flow fluctuations, yielding inconsistent and unreliable results, and will not be presented. Figure 5 shows a closer view of the sensor located near the outer wall of the tunnel at station 2. The platform is traversed by the forward cable, which rides over a motor-driven pulley. A digital encoder is connected to the shaft of the pulley to indicate the position of the platform. The accuracy of the position measurement was within ± 0.64 cm (± 0.25 in.). A signal cable is looped around the rear stabilizing cable to provide data transfer from the sensor to the data-acquisition unit. The drive mechanism was arbitrarily mounted on either the inner or outer tunnel wall, depending on tunnel station. The

platform could be traversed to approximately 0.5 m (1.5 ft) of the wall on which the drive mechanism was mounted and to approximately 0.3 m (1.0 ft) of the opposite wall.

PRESENTATION OF RESULTS

The results and discussion are presented according to the following outline:

	Figure
Typical flow-sensor calibration	4
Repeatability of velocity-profile measurement	6
Horizontal velocity profiles	7
Composite horizontal velocity profiles	8 to 10
Vertical velocity profiles	11
Composite vertical velocity profiles	12 to 14
Flow-control vane with trailing-edge flap installed	15
Effect of flow-control-vane trailing-edge flaps on horizontal velocity profiles	16
Composite horizontal velocity profiles with trailing-edge flaps on flow-control vanes	17 to 19

DISCUSSION OF RESULTS

Mean Horizontal and Vertical Velocity Profiles

Repeatability of velocity-profile measurement.- Repeat velocity-profile measurements were obtained at three different tunnel stations to determine the accuracy of the overall profile measurement. These results are presented in figures 6(a), (b), and (c) for stations 13 (vertical), 17 (horizontal), and 18-1 (vertical), respectively; the test-section configuration and speed are indicated in each figure. For all three measurement stations, the second traverse compares favorably with the first traverse, which indicates essentially the same overall velocity profile. The velocity-ratio value at each measurement point for the second traverse does not exactly repeat the value measured during the first traverse. This difference was attributed mainly to unsteady flow, in addition to the accuracy and flow-direction sensitivity of the flow sensor. However, the precise measurement of the absolute flow velocity was not the purpose of this investigation. Instead, a representation of the overall flow characteristics (attached or separated, symmetric or unsymmetric) at each station of interest was desired and, as indicated by the velocity profiles in figure 6, this requirement was met with the aforementioned equipment.

Horizontal velocity profiles.- The horizontal velocity profiles around the baseline tunnel circuit are presented in figure 7 for a test-section dynamic pressure of

2.78 kPa (58 psf). This corresponds to about one-half the maximum capable operating condition for the tunnel, which is a very common testing condition.

Figure 7(a) shows the horizontal velocity profile at station 1. The abscissa is the lateral distance y , which is measured from the inner tunnel wall and is non-dimensionalized by the tunnel width w at the same station. The ordinate is the local measured flow velocity u , which is nondimensionalized by the maximum local flow velocity u_{\max} measured during this particular traverse. The velocity profile at the aft end of the closed test section (station 1) is uniform, thus giving an almost constant mean flow speed across this section. (See fig. 7(a).) The boundary-layer thickness (defined as $u/u_{\max} < 0.99$) at the inner wall is larger than at the outer wall. At the limit of the traversing mechanism, no falloff of the uniform-velocity region was detected at the outer wall.

The velocity profile at the entrance to the first diffuser (station 2) is presented in figure 7(b) for the closed test-section (CTS) and the open test-section (OTS) configurations. The uniform region is larger for the CTS than the OTS configuration. (A slight asymmetry exists for both configurations.) This is mainly due to the more rapid growth of the shear layer on the free jet in the OTS configuration. This results in much thicker boundary layers for the OTS configuration and presents a potential problem because diffuser performance is dependent on the inflow conditions. At the end of the first diffuser (station 8), the velocity profiles for both the CTS and OTS show a slight flow displacement toward the outer wall. (See fig. 7(c).) The exact cause of this effect is unknown. However, it is postulated that the unsymmetric boundary-layer growth present at stations 1 and 2 is further aggravated by the upstream effect of the first-corner turning vanes. In a more normal sense, as the flow approaches the first corner, it encounters the innermost turning vanes first. This presents an area of relatively high resistance compared with the outer portion of this flow front, hence causing a natural migration toward the outer wall.

Downstream of the first corner there are five flow-control vanes (FCV), which incorporate symmetric airfoils with split trailing edges. The function of the FCV is to constrict the airflow when the split trailing edges are opened. This provides a low test-section speed while maintaining a high fan rotational speed, which is more accurately controlled. The velocity profile at station 9, just downstream of these FCV's, is shown in figure 7(d). This station is located at the beginning of the second diffuser. The difference in the velocity ratio u/u_{\max} at the inner wall relative to the outer wall has increased compared with the velocity profile of station 8 (fig. 7(c)), thus resulting in a reduced velocity along the inner tunnel wall. This is the case for both the CTS and OTS configurations. The major difference between the CTS and OTS configurations is in the middle, high-velocity region of the velocity profile. The CTS configuration has a higher velocity near the outer edges of the high-velocity region. The two deficits in the velocity profiles ($y/w = 0.5$ and 0.7) are at points where the measurement happened to be directly behind two FCV's. At the end of the second diffuser (station 10), the airflow has essentially the same characteristics as those of station 9. (See fig. 7(e).) This is probably due to the fact that the second diffuser has parallel sidewalls with a divergent floor and ceiling. Therefore, the expansion is only in the vertical plane.

After the flow turns the second corner, the velocity falls off rapidly along the inner walls, as indicated by the velocity profile for station 11. (See fig. 7(f).) This, again, may be attributed mainly to the effect of the turning vanes at the second corner, as discussed previously for the first corner. The velocity profile for the CTS configuration is fuller than that for the OTS configuration. At the

midpoint of the third diffuser (station 12), the flow has separated from the inner wall as indicated by the region of zero velocity shown in figure 7(g). This separation is caused by the relatively low velocity along the inner walls ahead of this station (stations 10 and 11). In addition, the flow along the inner wall must execute a 90° turn through the second corner plus a 5° third-diffuser angle. This low-energy flow is unable to execute the 95° turn. Figure 7(h) shows the velocity profile at station 13, which is located at the end of the third diffuser. This is also the entrance to the drive-fan section. Although the separated region present at station 12 (fig. 7(g)) appears to have reattached, the velocity profile is highly skewed toward the outer wall. This results in an unsymmetric loading of the drive fan. The large deficit in the center of the velocity profile shown in figure 7(h) is the upstream effect of the fan-hub fairing.

At the beginning of the fourth diffuser (station 14), which is downstream of the drive section, the velocity peak near the outer wall has become substantially larger than the peak near the inner wall. (See fig. 7(i).) This sets up an undesirable velocity gradient in the lateral direction. The velocity ratio along the inner wall has increased from about 20 percent of the maximum at station 13 (fig. 7(h)) to about 50 percent of the maximum at station 14 (fig. 7(i)). The velocity deficit in the middle of figure 7(i) is caused by the wake of the nacelle, which encloses the drive motors.

The velocity profile midway through the fourth diffuser (station 15) is shown in figure 7(j). The two velocity peaks at station 14 (fig. 7(i)) have merged to form one peak at station 15. The portion of the velocity profile near the outer wall is very unsteady compared with the portion near the inner wall, which is indicative of incipient flow separation. At the end of the fourth diffuser (station 16), the flow has completely separated from the outer wall. (See fig. 7(k).) There is actually a large zone (from $y/w = 0.8$ to 1.0) of reversed (upstream) flow, as indicated by the region of negative values of u/u_{\max} in figure 7(k) and supported by visual observations of the sensor. It is postulated that this flow reversal is caused by the asymmetric velocity distributions in conjunction with the large diffusion angle ($\approx 4^\circ$) of the fourth diffuser, and it is further complicated by the change in shape from circular to rectangular. This zone of reverse flow persists back to the third corner of the tunnel as evidenced by tufts and smoke observations. As shown by the velocity profile after the third corner (station 17), the flow reattaches to the outer wall. (See fig. 7(l).) The flow has become more symmetric at station 17 than at the stations upstream. The velocity profile at this station indicates that there is no core flow, which is to be expected in this region of the tunnel without some form of boundary-layer control.

The velocity profile downstream of the fourth corner (station 18) shows that the flow becomes slightly skewed toward the outer wall. (See fig. 7(m).) A similar trend existed for the first and second corners. The flow velocity along both the inner and outer walls and the fullness of the velocity profile increase as the flow passes through the 200 short-chord turning vanes on the fourth corner.

The effect of the two turbulence-reduction screens on the airflow can be seen in figure 7(n), which shows the velocity profile at station 19. The velocity ratio along each wall is above 70 percent of the maximum at this station. In addition, the overall velocity profile is more uniform in comparison with the profile upstream of the screens at station 18. These effects are due in large part to the pressure drop across the two screens. Each screen provides a 0.05-kPa (1-psf) pressure drop. The velocity deficit located at $y/w = 0.48$ indicates an imperfection in either or both of the screens. However, upon visual inspection of the screens in this region, no

large imperfections could be ascertained. Thus, the reason for this deficit is currently unknown. The effect of the contraction is shown by the velocity profile at station 20. (See fig. 7(o).) This station is located near the end of the contraction, just upstream of the test section. The contraction has an extremely powerful effect, taking a profile similar to that of figure 7(n) and converting it to the profile shown in figure 7(o).

Composite horizontal velocity profiles.- Composite horizontal velocity profiles are presented in figures 8 through 10. These figures show the mean velocity profiles around the entire tunnel circuit for test-section dynamic pressures of 1.53, 2.78, and 4.79 kPa (32, 58, and 100 psf, respectively) for both the closed and open test-section configurations. Figures 8(a) and (b) present the horizontal velocity profiles at $q_{TS} = 1.53$ kPa (32 psf) for the CTS and OTS configurations, respectively. As previously presented for the case with $q_{TS} = 2.78$ kPa (58 psf), the only significant differences between the CTS and OTS configurations are for stations 2 through 11. At station 2, the CTS configuration has very small boundary layers compared with the OTS configuration. Thus, the CTS configuration has a more extensive region of uniform flow. At stations 8 through 11, the CTS configuration generally has a fuller velocity profile in comparison with that of the OTS configuration. For stations 12 through 20, the differences between the CTS and OTS configurations are very slight. Figures 9(a) and (b) show the velocity profiles at $q_{TS} = 2.78$ kPa (58 psf) for the CTS and OTS configurations, respectively. Figure 10 shows the velocity-profile distribution around the tunnel circuit at $q_{TS} = 4.79$ kPa (100 psf) for the CTS configuration. This dynamic pressure is beyond the capabilities of the OTS configuration. The trends exhibited at this dynamic pressure are similar to those at the two pressures presented previously.

Vertical velocity profiles.- Vertical velocity profiles were measured at stations 10, 11, 13, 15, 16, and at three lateral locations at station 18. These are presented in figure 11 for the same conditions as those for the horizontal velocity profiles discussed earlier.

The vertical velocity profile at station 10 is shown in figure 11(a). The non-dimensionalized velocity in this case is plotted against the vertical distance above the tunnel floor z , which is nondimensionalized by the tunnel-circuit height h at this station. The CTS configuration has a fuller velocity profile than the OTS configuration. However, both velocity profiles are fairly symmetric about the tunnel center line ($z/h = 0.5$). After the flow turns through the second corner, the symmetry of the velocity distribution is lost, as indicated by the velocity profiles at station 11. (See fig. 11(b).) Again, the velocity profile for the CTS configuration is fuller than for the OTS configuration. The blockage effect of the debris-catching screen, which covers the lower third of the second-corner cross-sectional area, can be seen by the slight discontinuity in both the CTS and OTS velocity profiles near $z/h = 0.3$. At station 13 (fig. 11(c)), the difference between the CTS and OTS is less pronounced when compared with the previous two stations. In addition, the velocity profile is slightly skewed toward the ceiling. Midway down the fourth diffuser (station 15), the width of the core has narrowed. The boundary-layer thickness at the floor is larger than along the ceiling, as shown in figure 11(d). This situation persists until the end of the fourth diffuser (station 16). (See fig. 11(e).)

At station 18, vertical velocity profiles were measured at three lateral stations to provide a better understanding of the existing flow-field uniformity and to provide insight into the design of a honeycomb to be installed at or near this station. (See figs. 11(f) through (h).) The three lateral stations were 18-1 (at the center of the section), 18-2 (halfway between the center and outer wall), and 18-3

(halfway between the center and inner wall). All three profiles were similar in shape. However, the profile along the center of this section (station 18-1) was not as unsteady as the two off-center profiles. This can be seen by comparing figure 11(f) with figures 11(g) and (h).

Composite vertical velocity profiles.- Composite vertical velocity profiles are presented in figures 12 through 14 for the same conditions as the composite horizontal velocity profiles. Figure 12 shows the velocity profiles for the case with $q_{TS} = 1.53 \text{ kPa}$ (32 psf). Again, the velocity profiles are fuller for the CTS than for the OTS at stations 10 and 11. At station 13 and beyond, only slight differences exist between the CTS and OTS configurations. This was also the case for the horizontal velocity profiles, where similar trends and conclusions exist at values of q_{TS} of 2.78 kPa (58 psf) and 4.79 kPa (100 psf). (See figs. 13 and 14.)

Effect of FCV Trailing-Edge Flaps

Two major problems were discussed in the previous section pertaining to the tunnel-circuit flow characteristics: the unsymmetric flow upstream of the drive fan and the separated region of reversed flow in the fourth diffuser. The unsymmetric flow upstream of the drive fan is probably caused by the combination of asymmetric flow in the first and second diffusers in combination with the flow separation in the third diffuser. The area of flow reversal in the fourth diffuser is probably the result of distorted flow at the diffuser entrance in combination with the large diffusion angle and change in shape.

A conceivable solution to the first problem would be to install flow deflectors at an appropriate upstream location. The traditional approach has been to install extensions to corner turning vanes. This approach was not considered to be cost effective for this facility because of the large number of turning vanes (55 for the first corner and 55 for the second corner) in addition to the significant amount of tunnel shutdown time required for installation. Instead, it was decided that flow-deflector trailing-edge flaps would be designed and installed on each of the five existing FCV's. (See fig. 2.) As mentioned previously, the FCV's incorporate symmetric airfoils with split trailing edges. The design of these trailing-edge flaps was accomplished by using the NASA/Langley Multi-Component 2-D Viscous Airfoil program described in reference 7. This program has a feature which traces the position of the stagnation streamline due to a flap deflection. In addition, the point of possible separation, if any, is predicted. It was determined that a deflection of the flow 0.9 m (3 ft) closer to the inner wall would result in a nearly symmetric velocity distribution upstream of the drive fan. After evaluating several configurations, a flap geometry was determined that gave the desired flow deflection without predicted separation on the FCV. This configuration was a 0.46-m-chord (1.5-ft) trailing-edge flap deflected 25°. (See fig. 15.) These flaps were installed at low cost with minimal tunnel shutdown.

Horizontal velocity profiles with FCV trailing-edge flaps installed.- The effect of these flow deflectors on the velocity distribution at several stations (10, 12, 13, 14, and 16) in the aft leg of the tunnel is presented in figure 16. For the CTS configuration (station 10), the flow velocity along the inner wall has been increased from about 30 percent of the maximum velocity for the base-line tunnel to about 60 percent of the maximum velocity with the flow deflectors in place. (See fig. 16(a).) The velocity deficits due to the FCV's with flaps are more prevalent now because the symmetric FCV's have been converted to cambered surfaces with the

addition of the flow-deflector trailing-edge flaps. This resulted in higher drag and increased wake deficits in addition to a 6-percent increase in tunnel drive power at a test-section dynamic pressure of 2.78 kPa (58 psf). However, this is offset by the 33-percent reduction in tunnel drive power because of the removal of the dense debris-catching screen located at the second corner. There were initial concerns about inducing possible wall separation by overdeflecting the airstream; but, based on the results of the velocity profile at station 10, this does not appear to be the case. Similar characteristics exist for the OTS configuration at this station. (See fig. 16(b).)

At station 12 (figs. 16(c) and (d)), the separated region along the inner wall that existed without the flow deflectors has been eliminated by the installation of the flow deflectors. Obviously, energizing the flow along the inner wall has allowed it to turn the large 95° angle, mentioned in the previous section, without separation. With the elimination of the separation bubble, the velocity profile at station 12 is almost perfectly symmetric. This trend continues through the third diffuser and results in a velocity profile at station 13 (figs. 16(e) and (f)), which is very symmetric with respect to the distorted velocity profile that existed at this station without the flow deflectors. Based on these results, the first of the two major flow problems appears to have been alleviated.

The improvements to the velocity distributions due to the flow deflectors continue downstream of the drive section, as indicated by the velocity profile at station 14. (See figs. 16(g) and (h).) With the flow deflectors, the velocity profile at this station has two velocity peaks of similar magnitude. However, without the flow deflectors, there was only one velocity peak on the outer portion of the tunnel and relatively low velocities on the inner portion. This result was not anticipated. Before the removal of the dense debris-catching screen on the second corner, the velocity profile upstream of the drive fan (station 13) was very similar to the data at this station with flow deflectors. (See ref. 5.) However, at station 14, the velocity profile was similar to the data at this station without flow deflectors. Therefore, it was assumed that even though the velocity distribution upstream of the drive fan could be improved by the use of flow deflectors, the flow downstream of the drive section would still be skewed and asymmetric. Apparently, a combination of replacing the dense second-corner screen and improving the velocity distributions results in flow improvements, which continue through the drive section into the fourth diffuser.

At the end of the fourth diffuser (station 16), the zone of reversed flow has been alleviated with the installation of the flow deflectors. (See figs. 16(i) and (j).) This effect was fortuitous because, as mentioned before, the flow deflectors were primarily designed to improve the flow upstream of the drive fan.

Composite horizontal velocity profiles with FCV trailing-edge flaps installed.- Composite horizontal velocity profiles for several stations (10, 12, 13, 14, and 16) in the aft leg of the tunnel are presented in figures 17 through 19. These are presented at values of q_{TS} of 1.53, 2.78, and 4.79 kPa (32, 58, and 100 psf, respectively) for both the CTS and OTS configurations with the FCV trailing-edge flaps installed. The results for the conditions presented are basically similar to those of the preceding section. There are slight differences, especially at station 16, for the case for $q_{TS} = 1.53$ kPa (32 psf) where the velocity falls off to essentially zero at the walls. (See fig. 17.) For the case for $q_{TS} = 4.79$ kPa (100 psf), the flow sensor malfunctioned during the velocity traverse at station 10, and the data were not obtained. (See fig. 19.) However, results similar to those of the other two cases would be expected.

CONCLUDING REMARKS

A series of investigations have been conducted to determine the mean flow characteristics throughout the circuit of the Langley 4- by 7-Meter Tunnel for test-section dynamic pressures of 1.53, 2.78, and 4.79 kPa (32, 58, and 100 psf, respectively). The velocity profile near the end of the closed test section (station 2) indicated a fairly uniform flow pattern. However, unsymmetrical flow patterns in the first, second, and third diffusers resulted in relatively low velocities along the inner wall of the tunnel. This caused flow separation midway through the third diffuser and resulted in a skewed velocity profile entering the drive fan. The skewed velocity profile, in combination with the large diffusion angle, caused flow separation along the outer wall of the fourth diffuser. This zone of separation can feed turbulent eddies into the airstream. Trailing-edge flaps were attached to the five flow-control vanes (FCV) to act as flow deflectors to displace the airstream and produce more symmetrical velocity distributions. These flow deflectors proved to be extremely effective in providing uniform flow entering the drive fan, thus alleviating the flow separation in the third and fourth diffusers.

The resulting improved base-line tunnel-circuit flow with the FCV flaps installed is now considered more suitable for the scheduled installation in 1984 of four screens and one honeycomb in the entrance to the contraction.

Langley Research Center
National Aeronautics and Space Administration
Hampton, VA 23665
October 3, 1983

REFERENCES

1. Harvey, William D.; Stainback, P. Calvin; and Owen, F. Kevin: Evaluation of Flow Quality in Two Large NASA Wind Tunnels at Transonic Speeds. NASA TP-1737, 1980.
2. Steinle, F.; and Stanewsky, E.: Wind Tunnel Flow Quality and Data Accuracy Requirements. AGARD-AR-184, Nov. 1982.
3. Mabey, D. G.: Flow Unsteadiness and Model Vibration in Wind Tunnels at Subsonic and Transonic Speeds. C.P. No. 1155, British A.R.C., 1971.
4. Paterson, Robert W.; Vogt, Paul G.; and Foley, William M.: Design and Development of the United Aircraft Research Laboratories Acoustic Research Tunnel. J. Aircr., vol. 10, no. 7, July 1973, pp. 427-433.
5. Barna, P. Stephen: Experimental Investigations on the V/STOL Tunnel at NASA/Langley Research Center. NASA CR-165655, 1981.
6. Kershner, David D.: Miniature Flow-Direction and Airspeed Sensor for Airplanes and Radio-Controlled Models in Spin Studies. NASA TP-1467, 1979.
7. Stevens, W. A.; Goradia S. H.; and Braden J. A.: Mathematical Model For Two-Dimensional Multi-Component Airfoils in Viscous Flow. NASA CR-1843, 1971.



L-81-5962

Figure 1.- The Langley 4- by 7-Meter Tunnel.

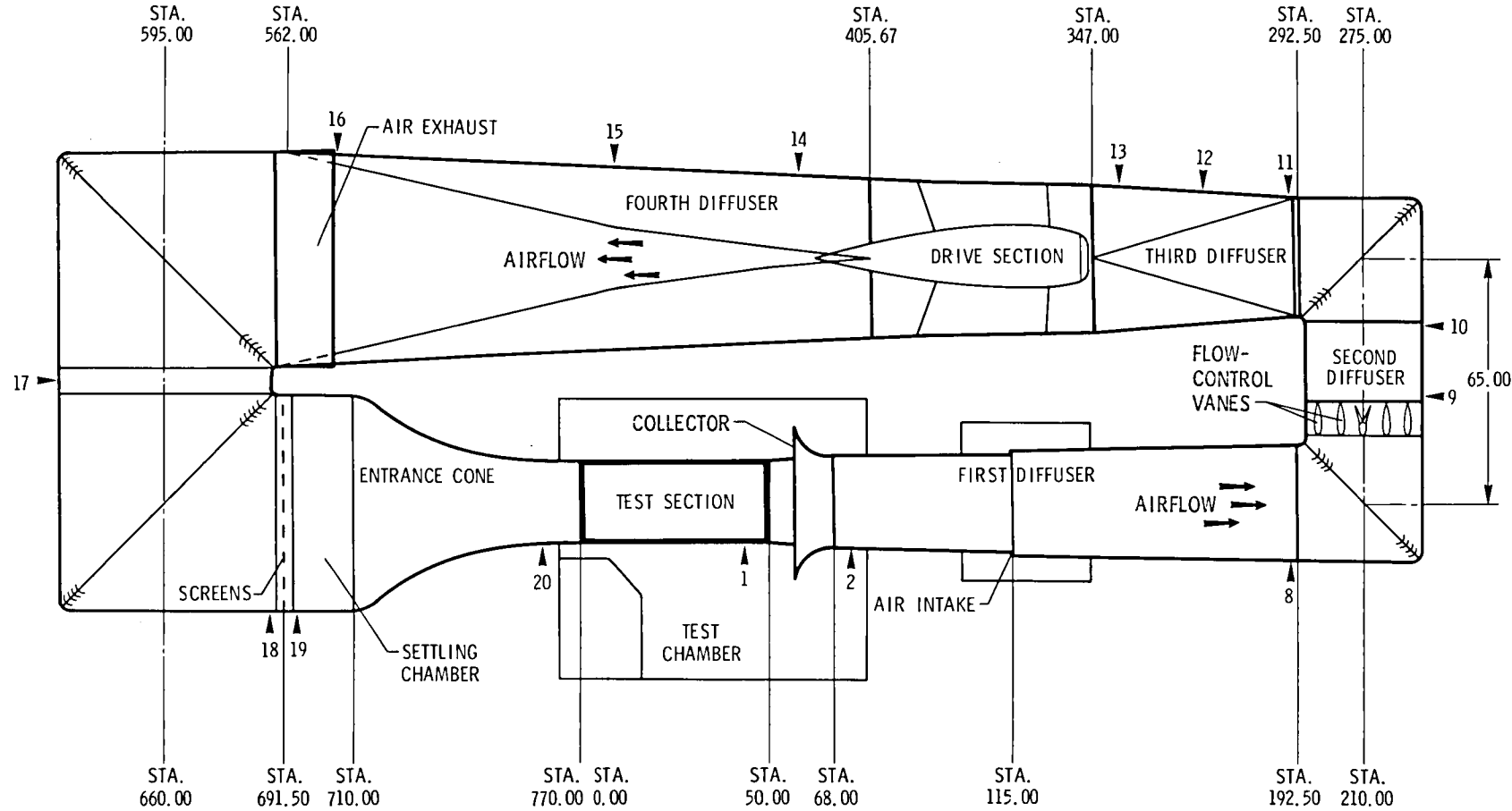
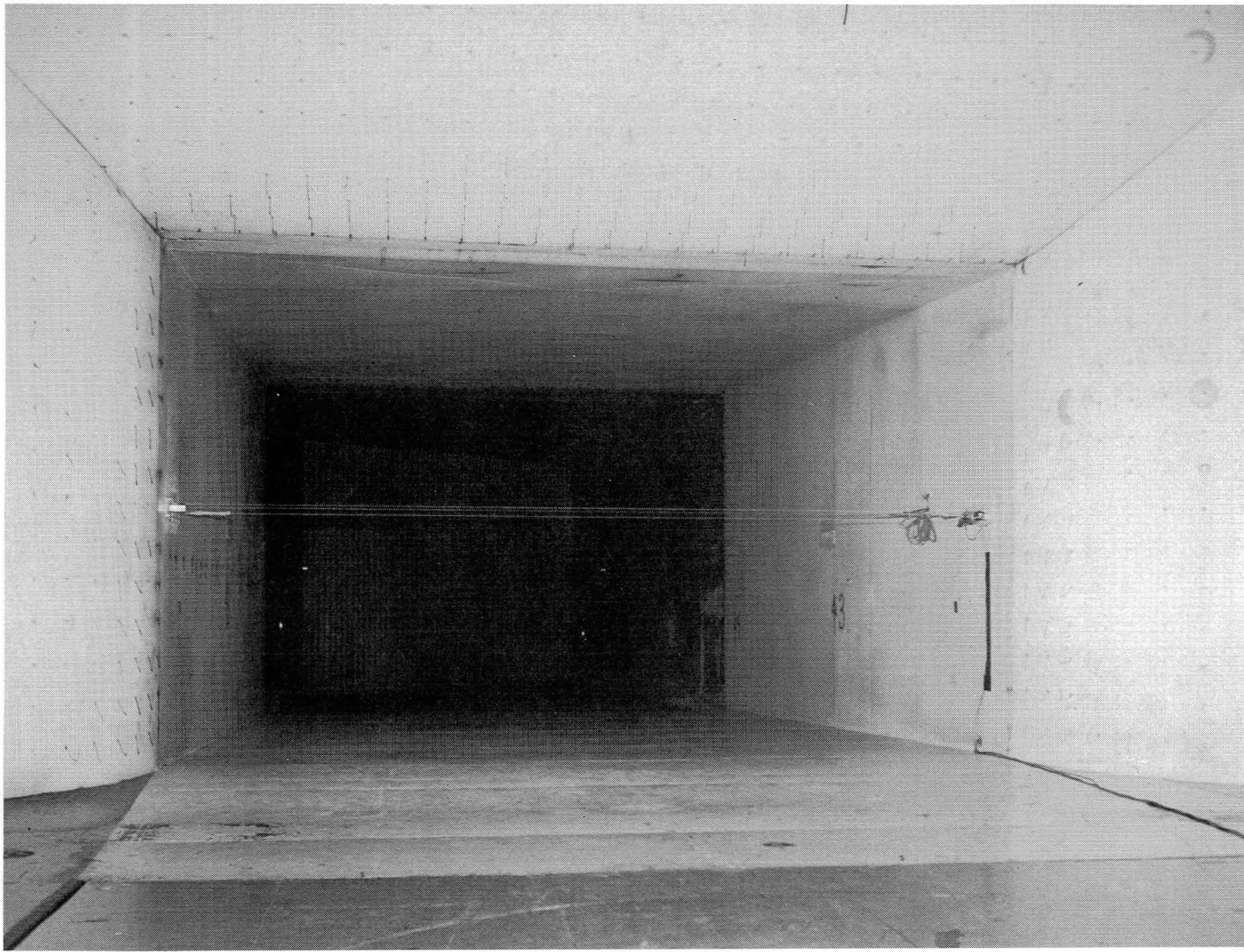
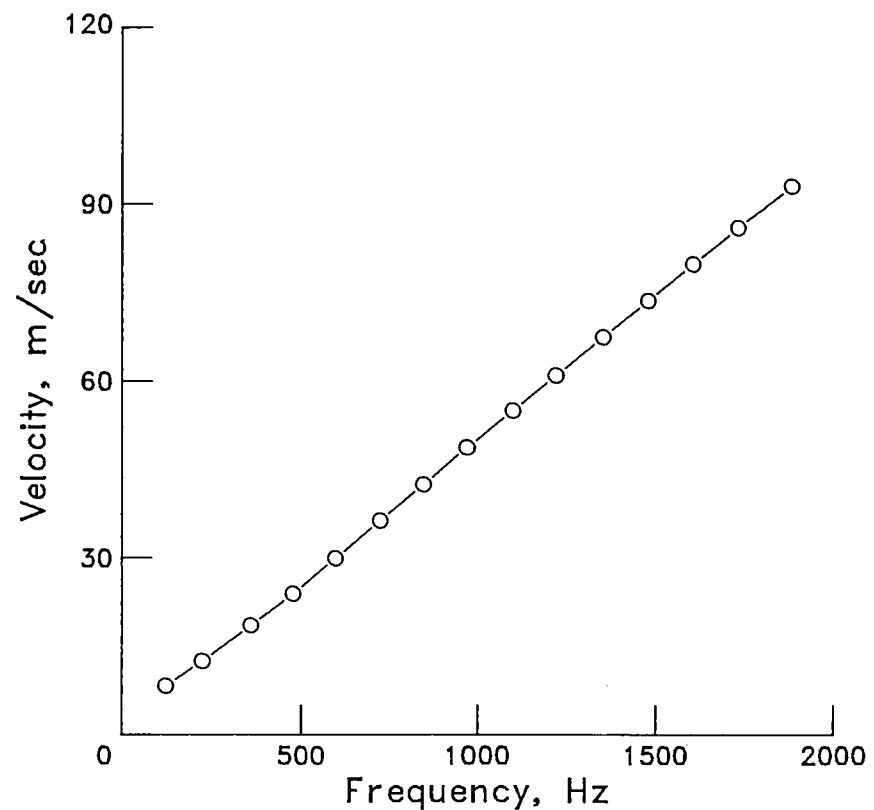
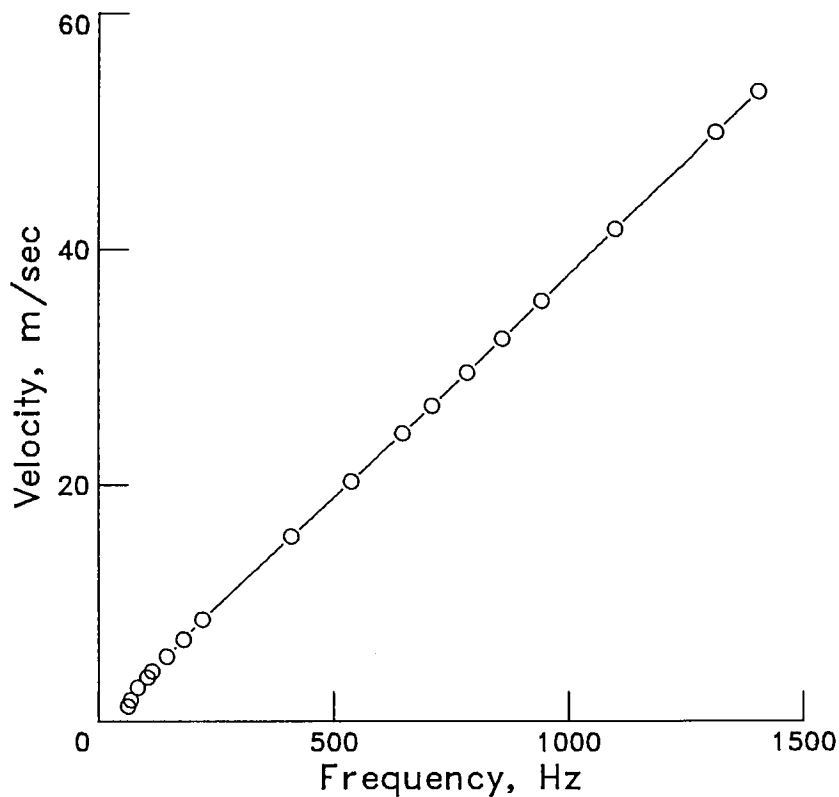


Figure 2.- Plan-view sketch of the Langley 4- by 7-Meter Tunnel showing velocity traverse stations.



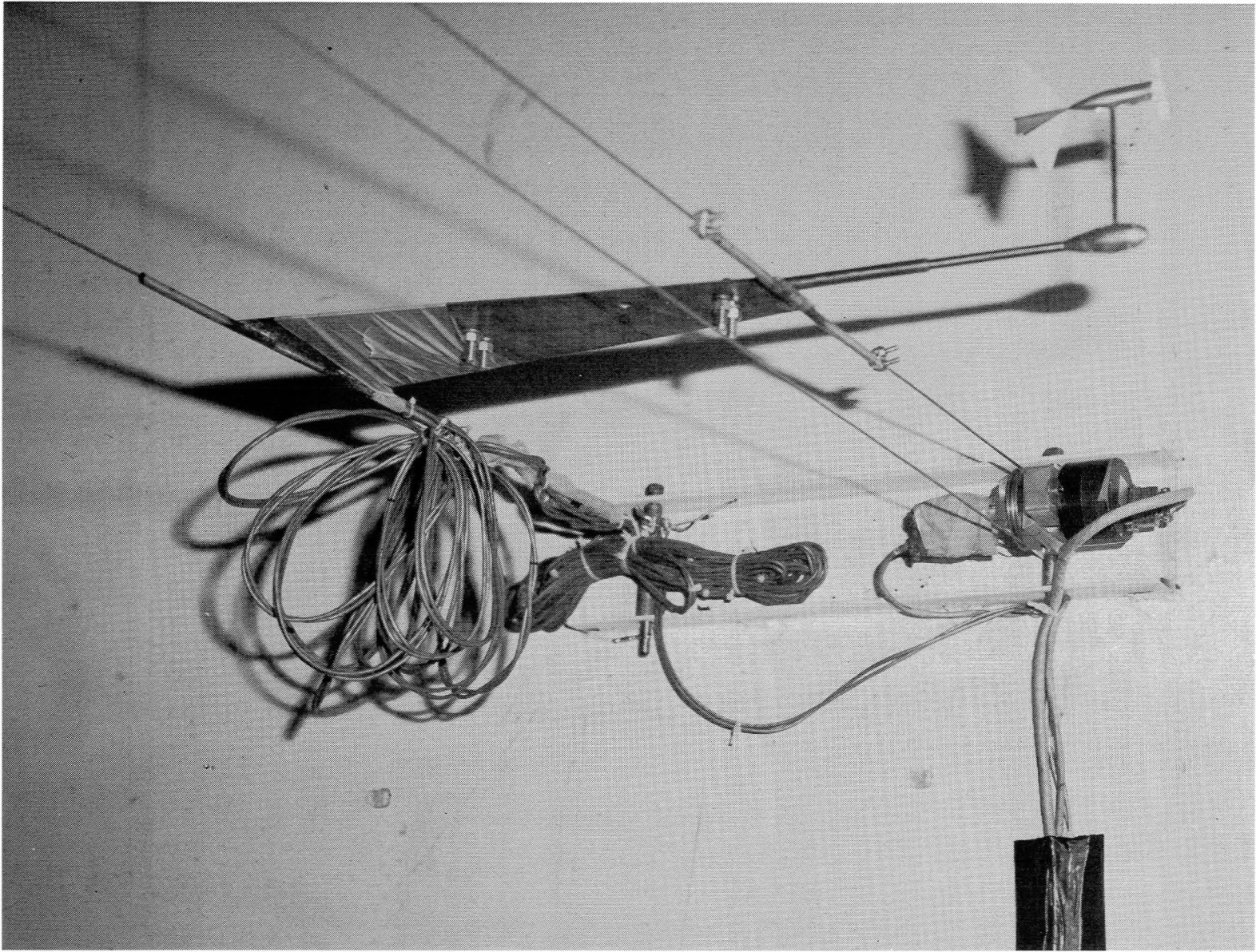
L-82-4004

Figure 3.- Setup for horizontal-velocity-profile measurements at station 2 for open test-section configuration.



(a) Low-speed propeller. 5.08-cm (2.00-in.) diameter. (b) High-speed propeller. 3.18-cm (1.25-in.) diameter.

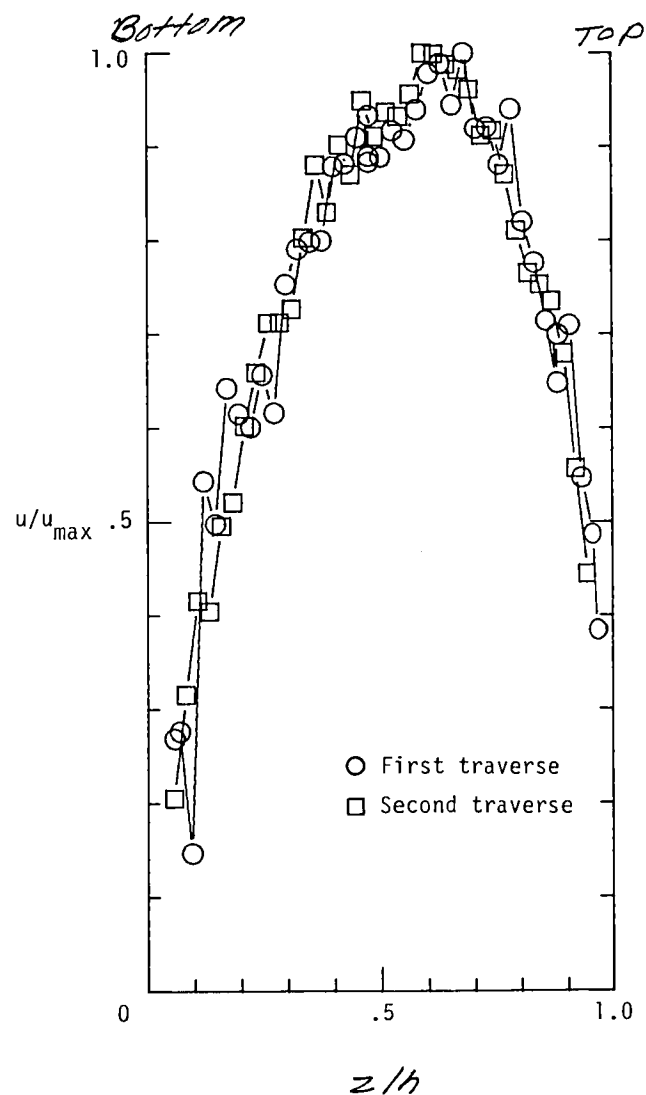
Figure 4.- Velocity calibration of propeller anemometer.



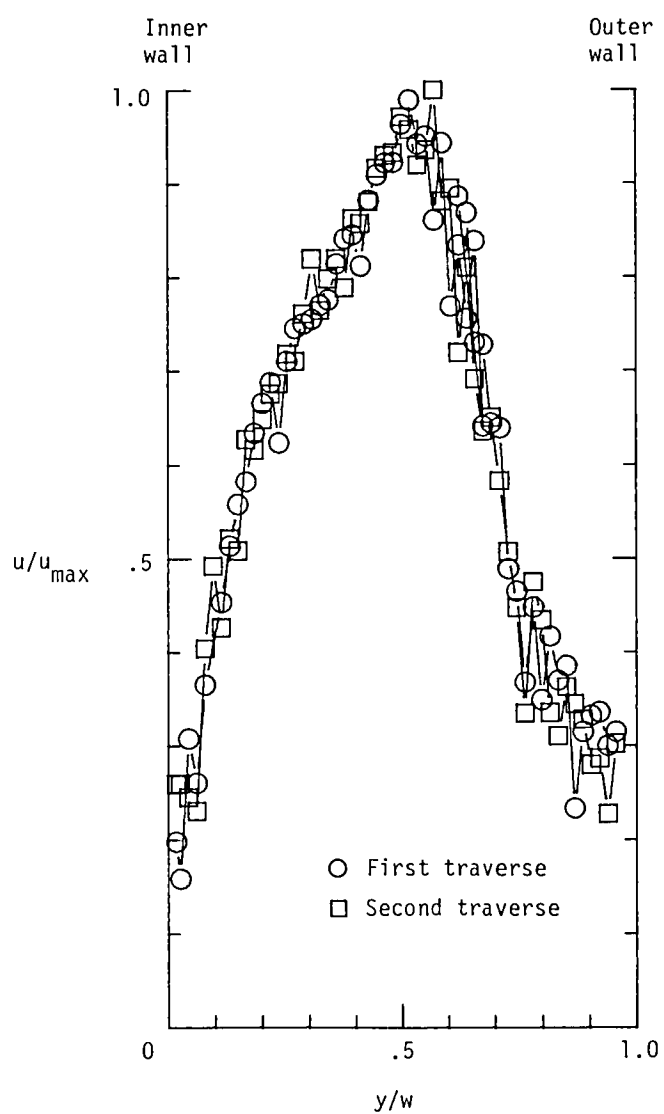
L-82-4005

Figure 5.- Flow sensor and traversing hardware located near outer wall.

*Erosion
1-3-84*

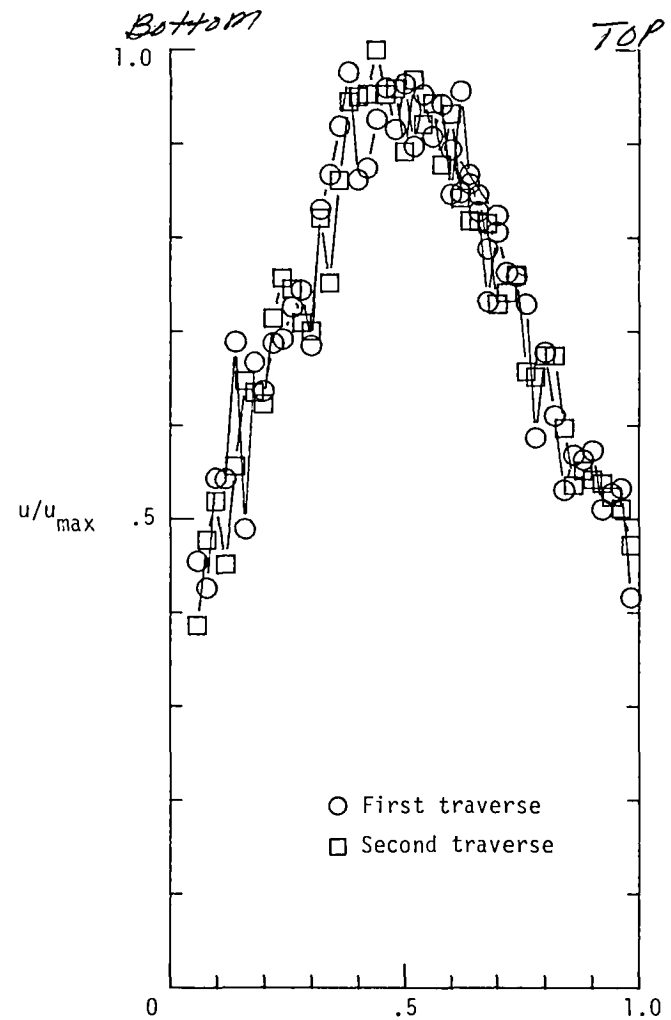


(a) Station 13 (vertical). Open test-section configuration; $q_{TS} = 2.78$ kPa (58 psf).



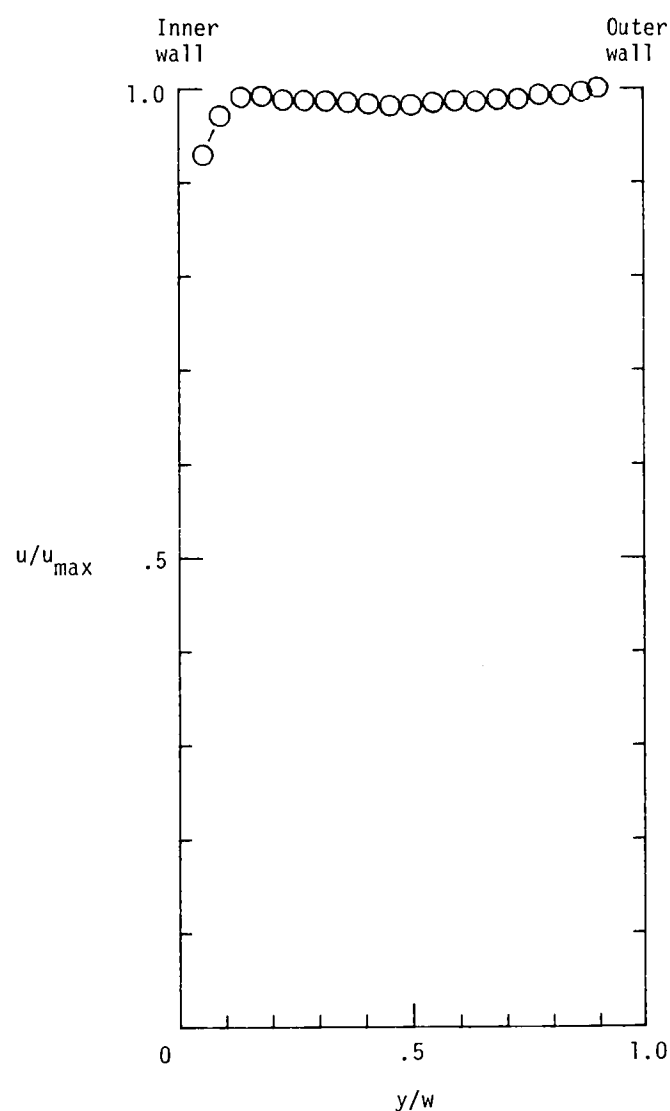
(b) Station 17 (horizontal). Closed test-section configuration; $q_{TS} = 4.79$ kPa (100 psf).

Figure 6.- Repeatability of velocity-profile measurement.

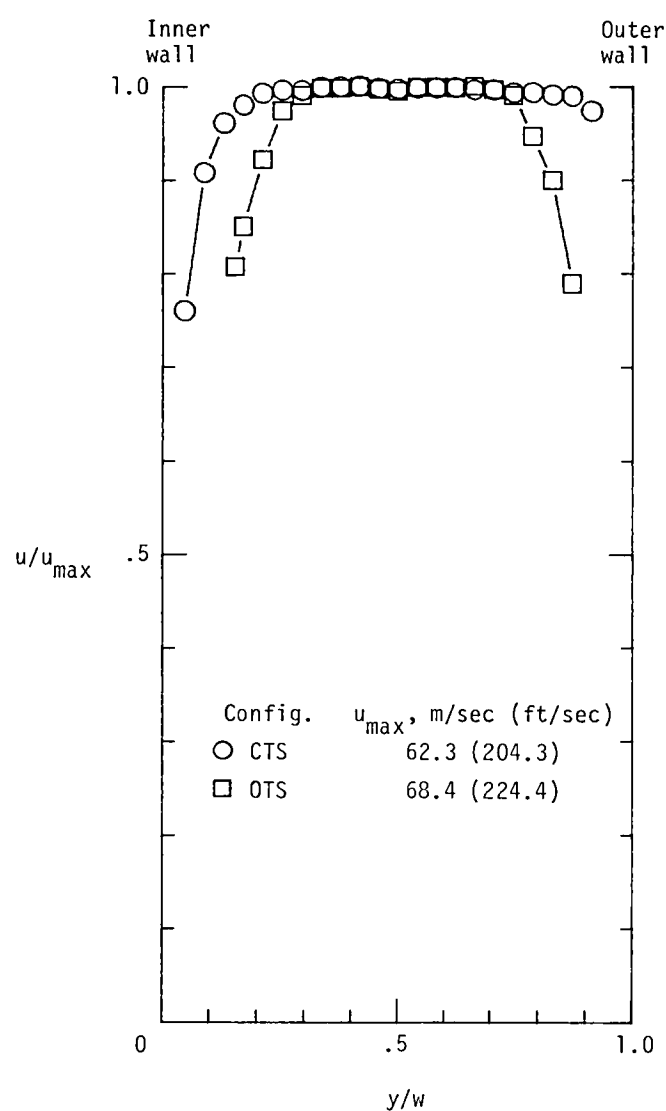


z/h
 (c) Station 18-1 (vertical). Closed test-section configuration; $q_{TS} = 4.79 \text{ kPa}$
 (100 psf).

Figure 6.- Concluded.

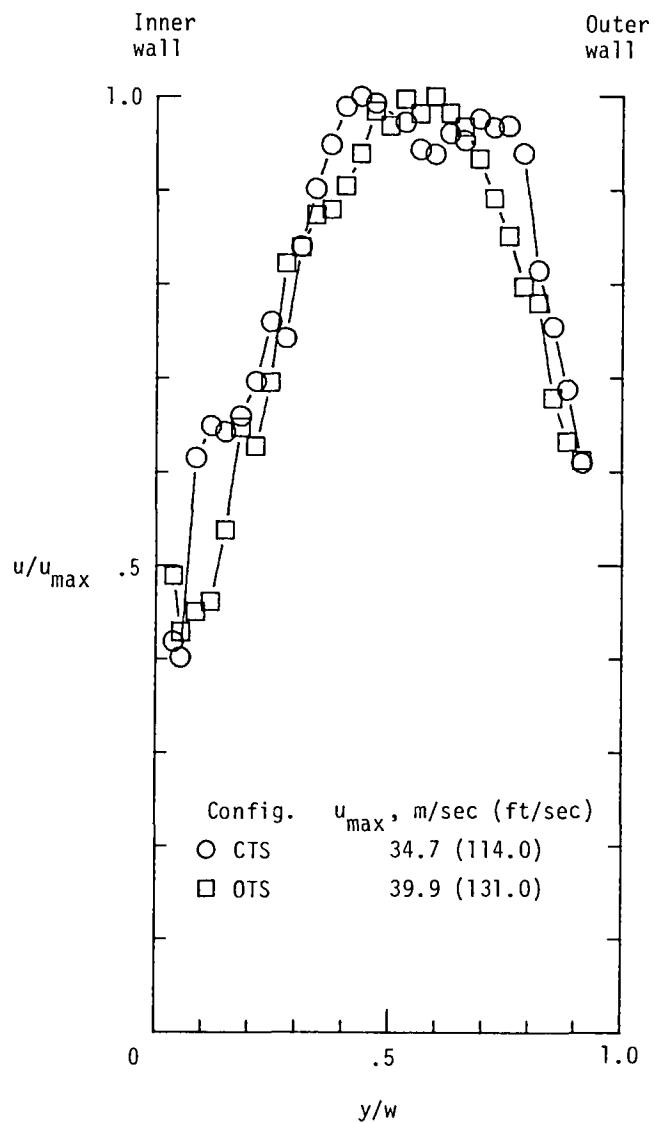


(a) Station 1. Closed test section;
 $w = 6.68 \text{ m}$ (21.92 ft); $u_{\max} = 68.2 \text{ m/sec}$
(223.7 ft/sec).

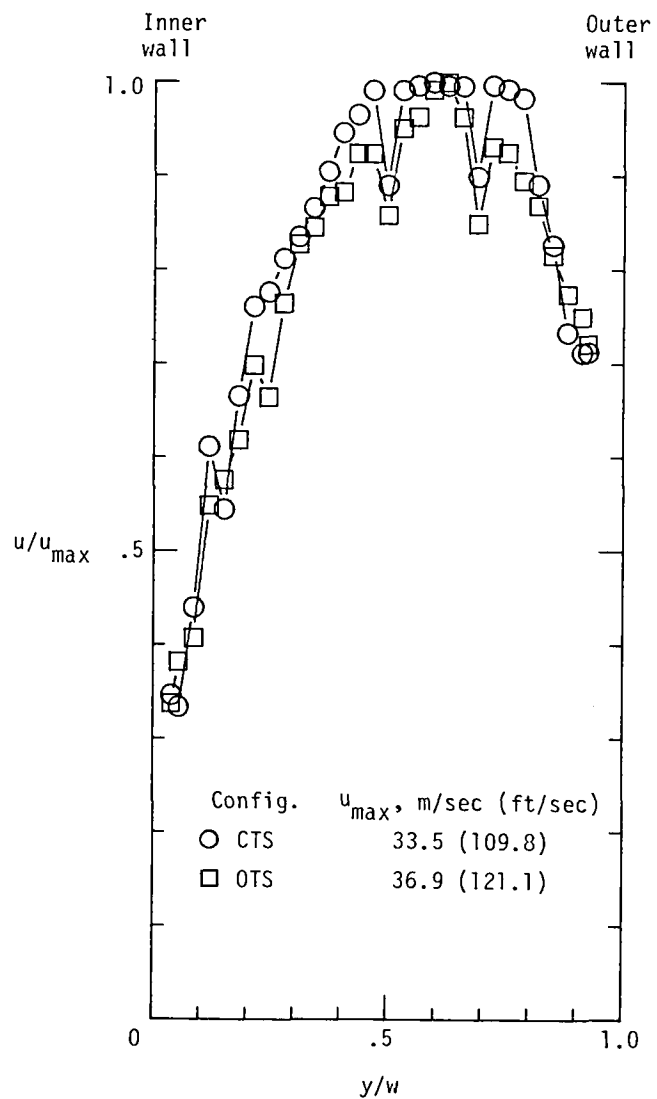


(b) Station 2. $w = 7.39 \text{ m}$ (24.25 ft).

Figure 7.- Horizontal velocity profiles at $q_{TS} = 2.78 \text{ kPa}$ (58 psf).



(c) Station 8. $w = 9.56$ m (31.38 ft).



(d) Station 9. $w = 9.59$ m (31.46 ft).

Figure 7.- Continued.

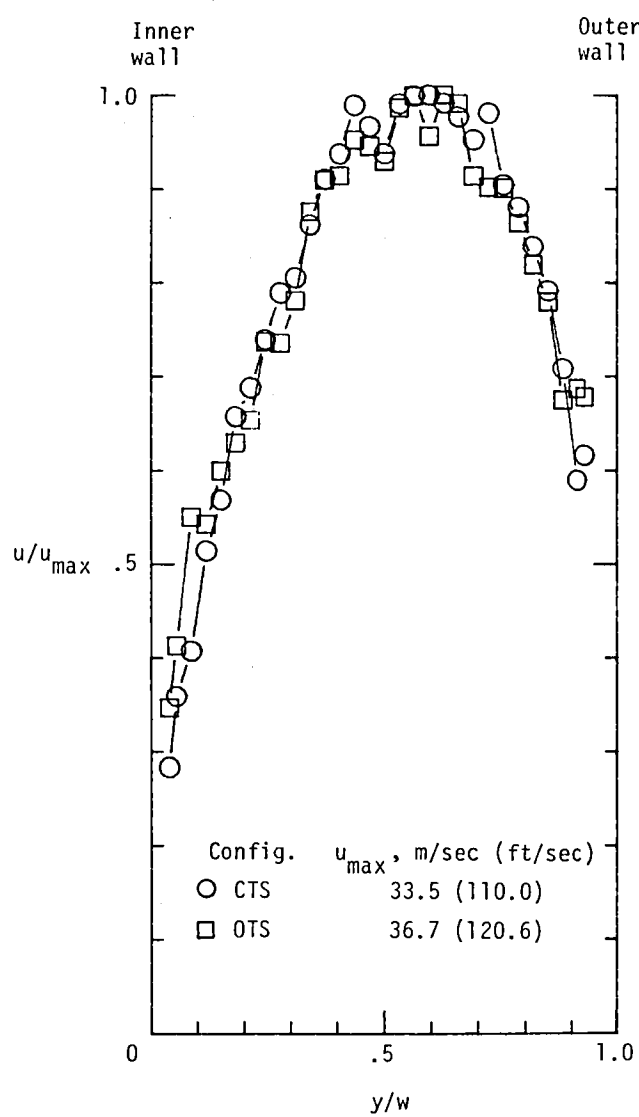
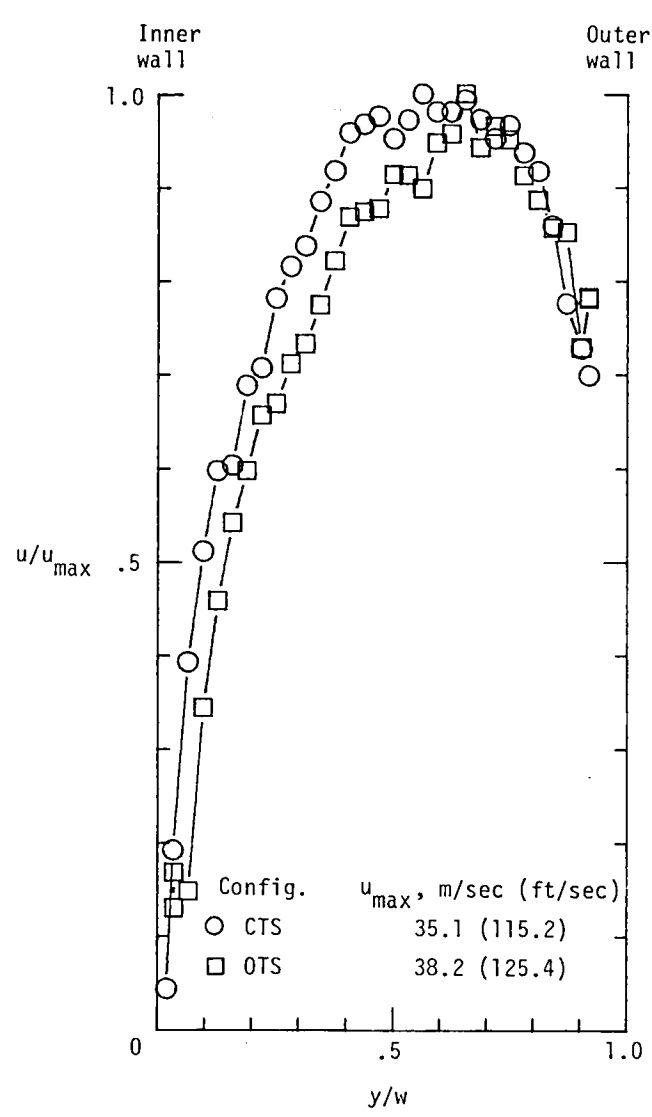
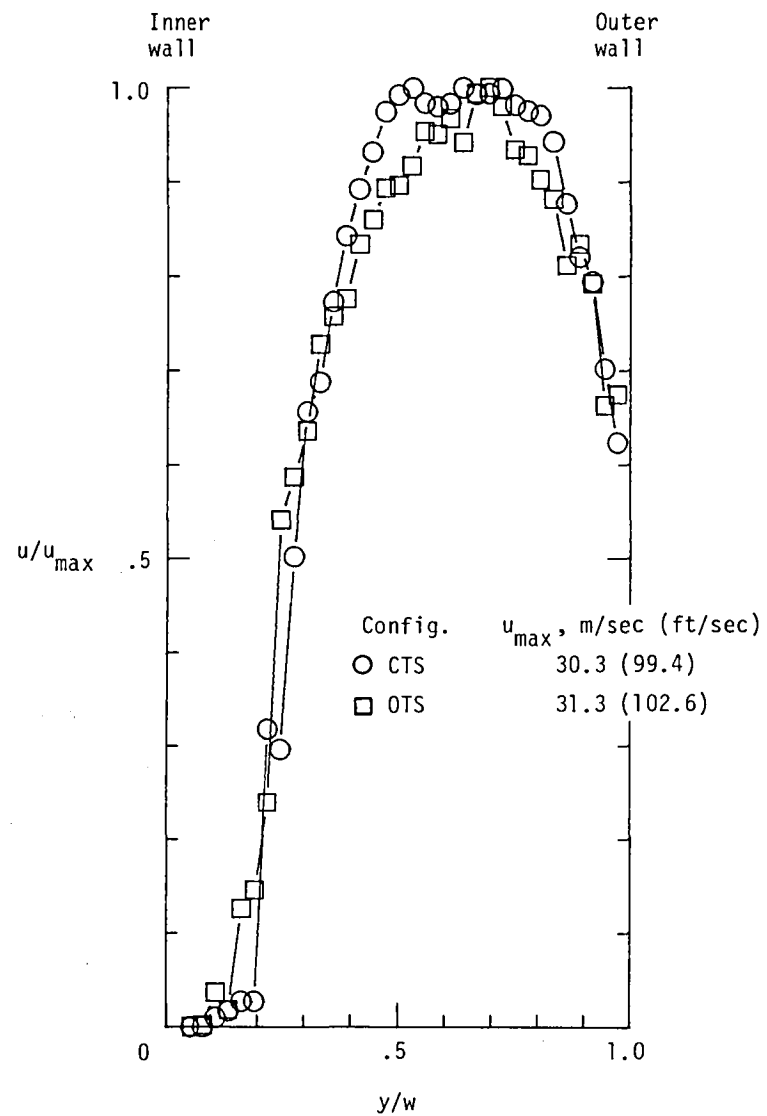
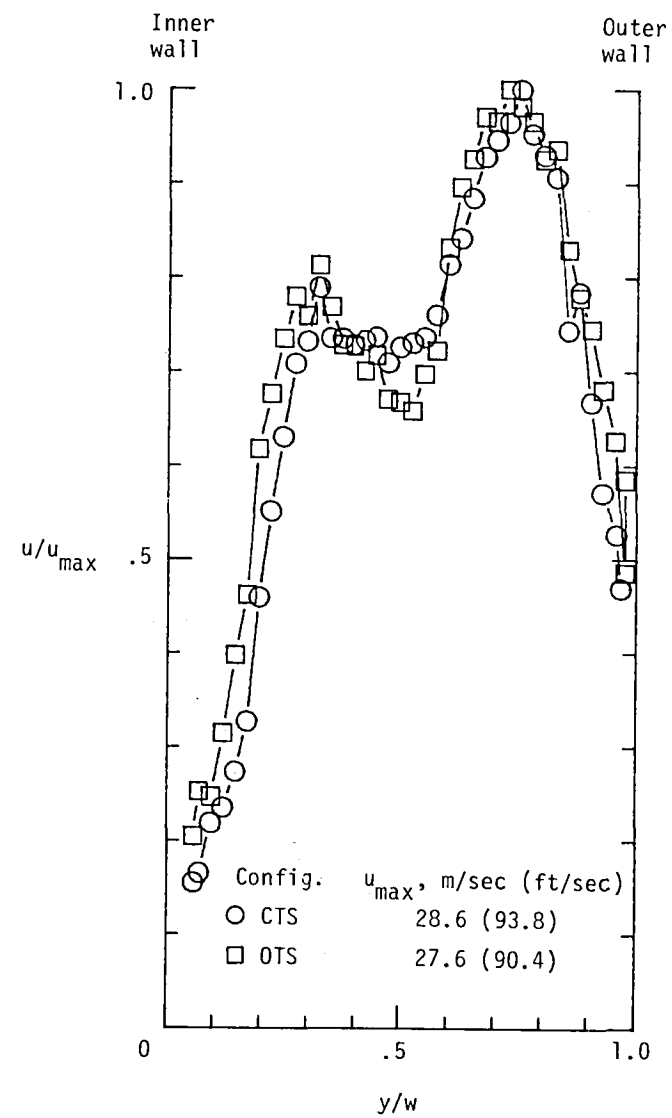
(e) Station 10. $w = 9.59$ m (31.46 ft).(f) Station 11. $w = 9.83$ m (32.25 ft).

Figure 7.- Continued.



(g) Station 12. $w = 11.0$ m (36.0 ft).



(h) Station 13. $w = 12.0$ m (39.5 ft).

Figure 7.- Continued.

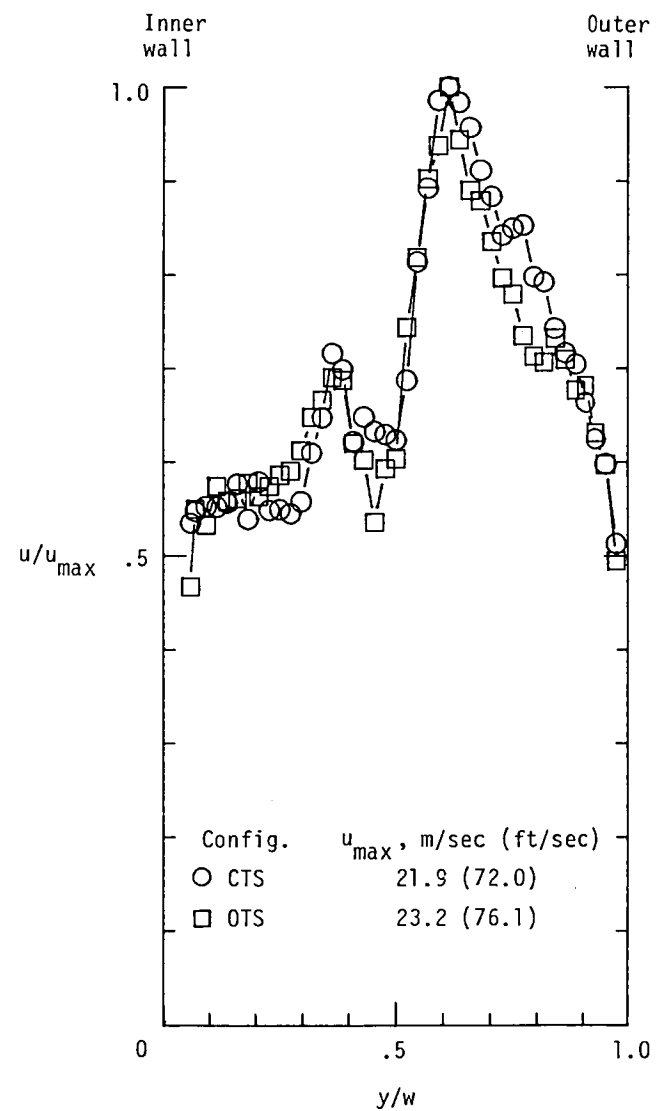
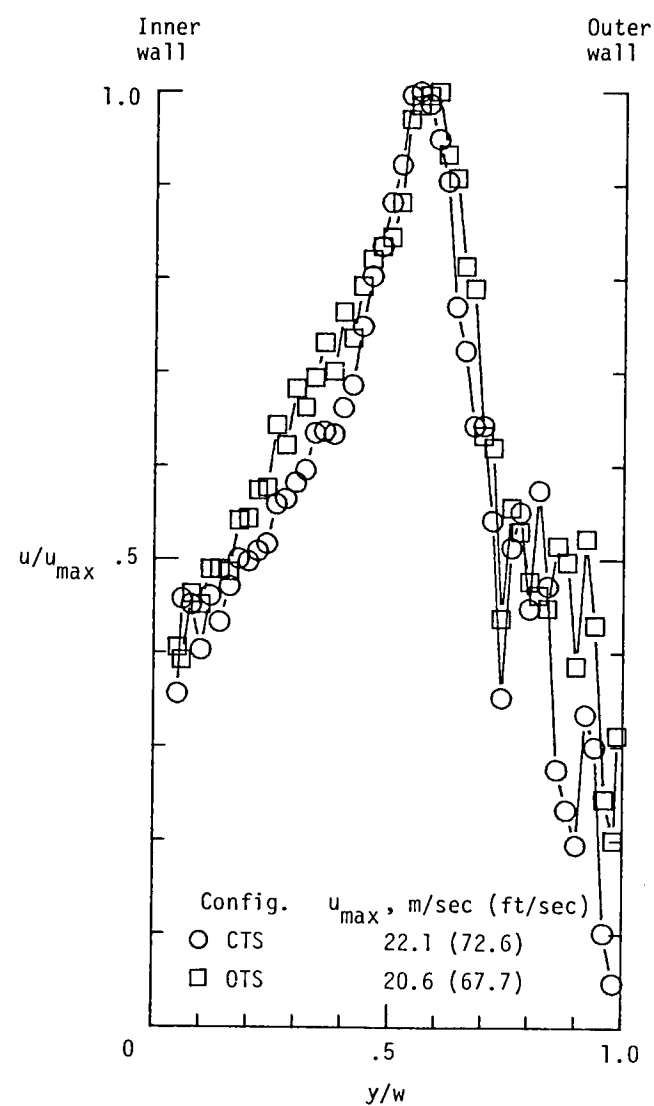
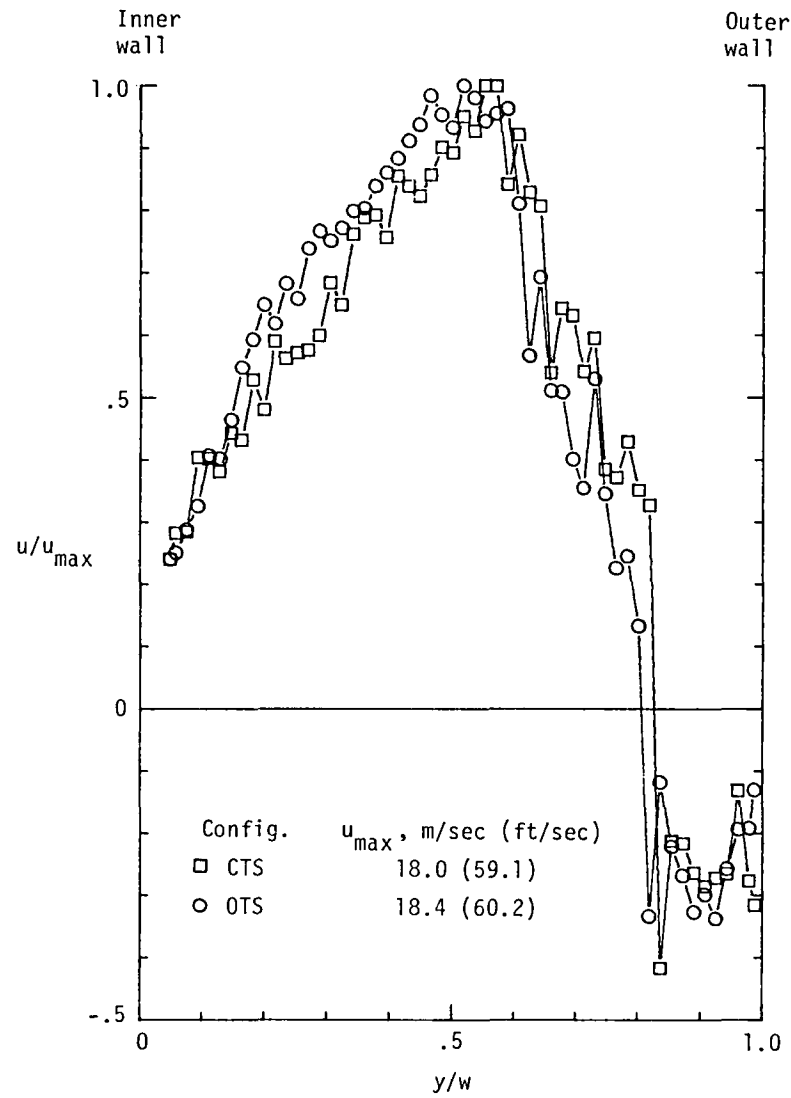
(i) Station 14. $w = 13.5$ m (44.25 ft).(j) Station 15. $w = 15.2$ m (50.0 ft).

Figure 7.- Continued.



(k) Station 16. $w = 17.2$ m (56.5 ft).

Figure 7.- Continued.

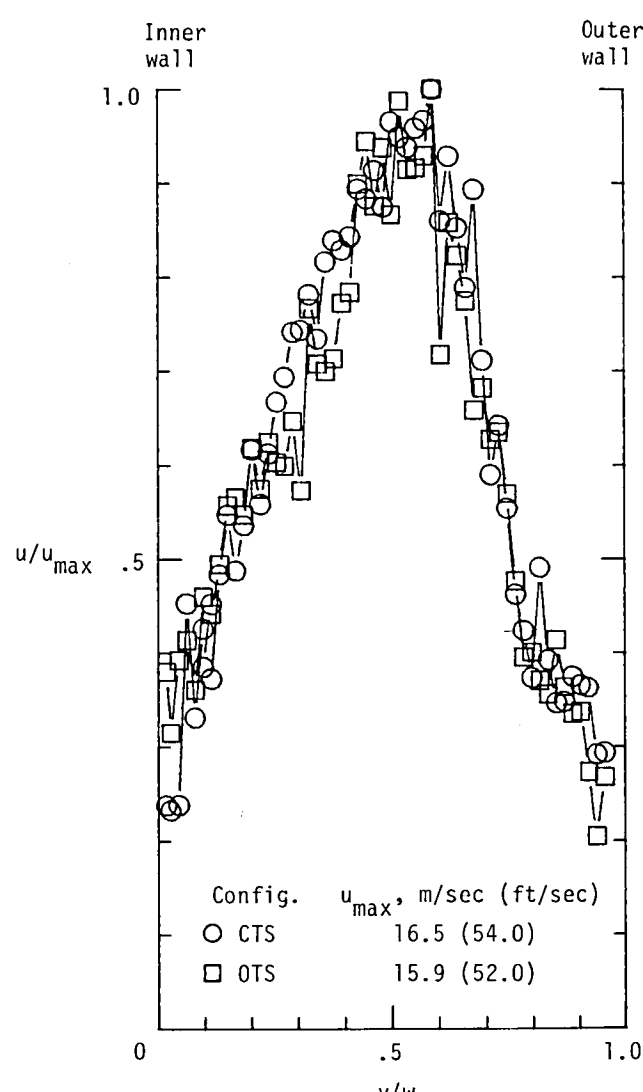
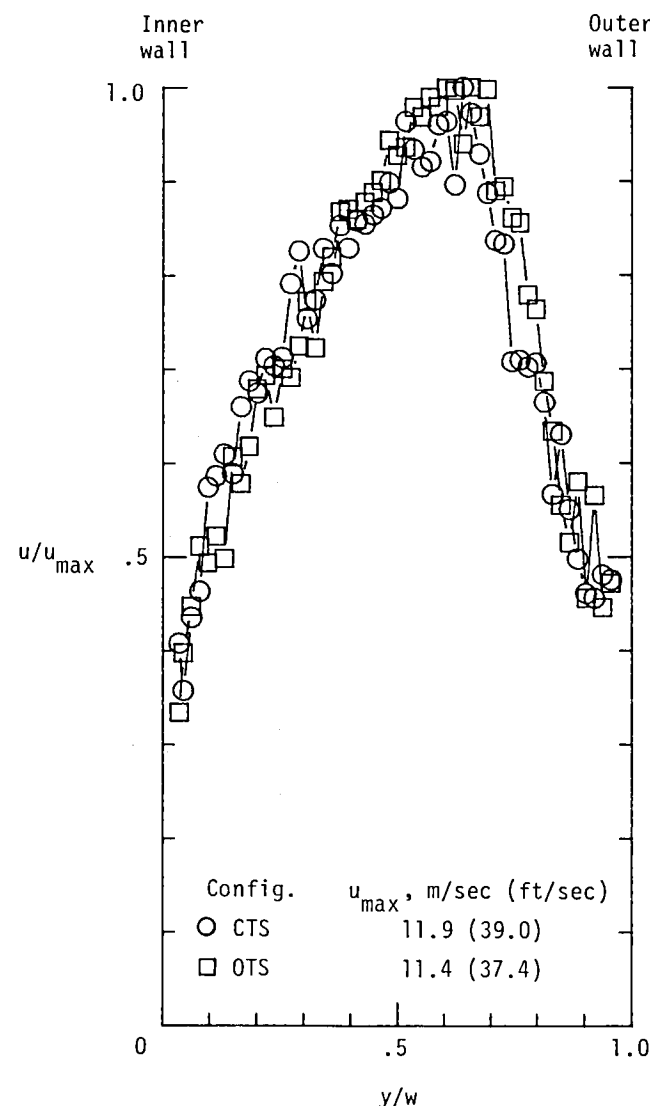
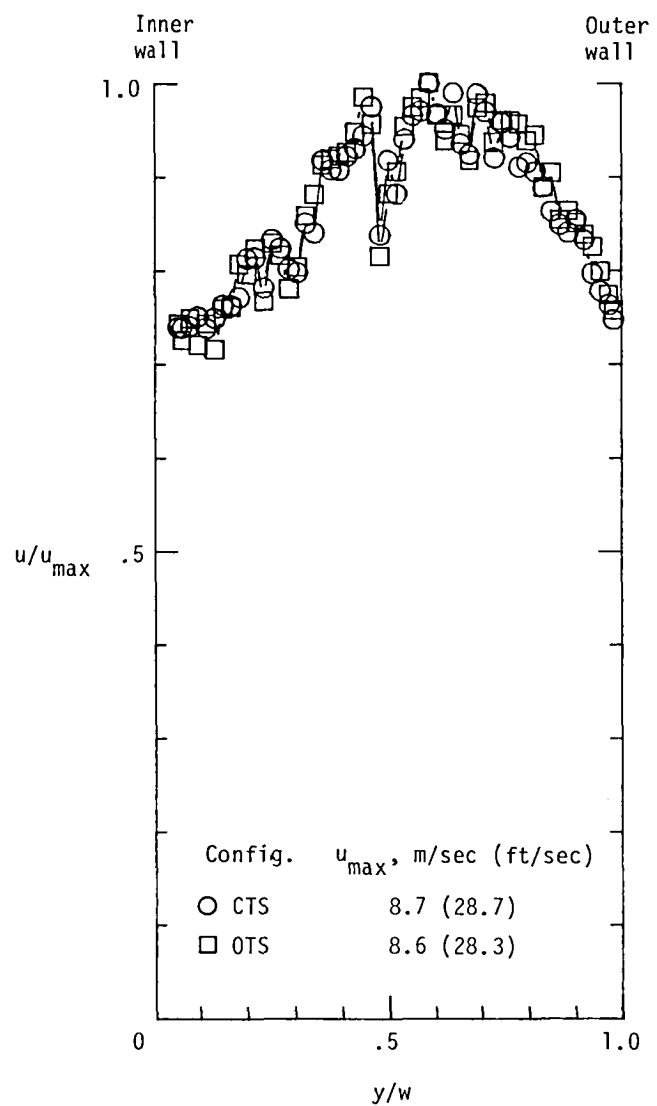
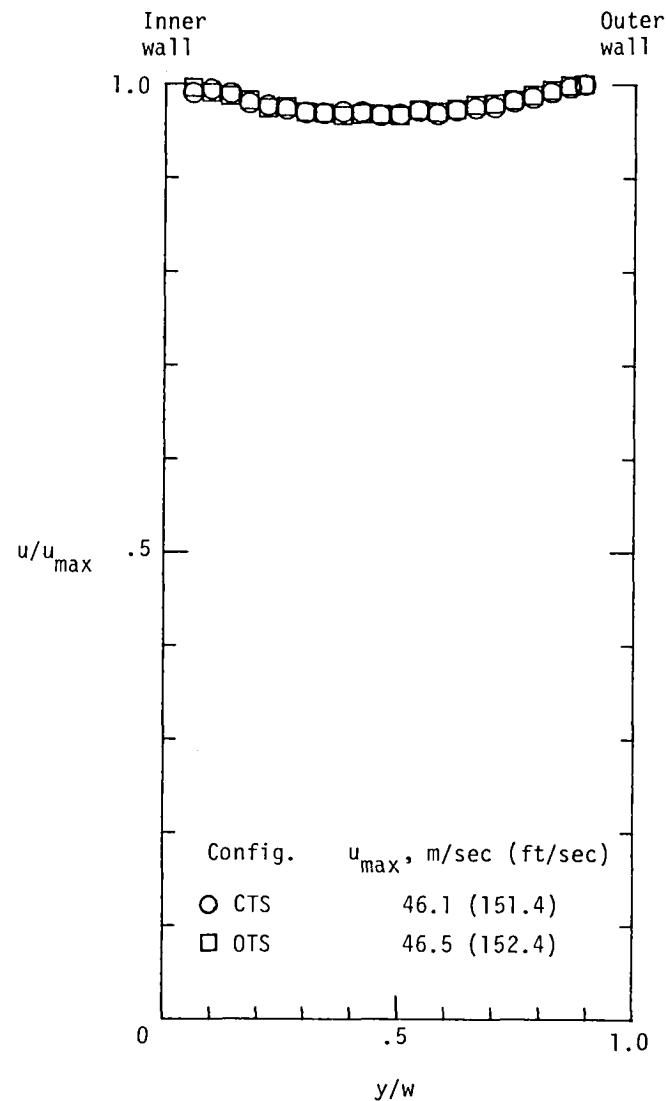
(l) Station 17. $w = 17.4$ m (57.0 ft).(m) Station 18. $w = 17.4$ m (57.0 ft).

Figure 7.- Continued.

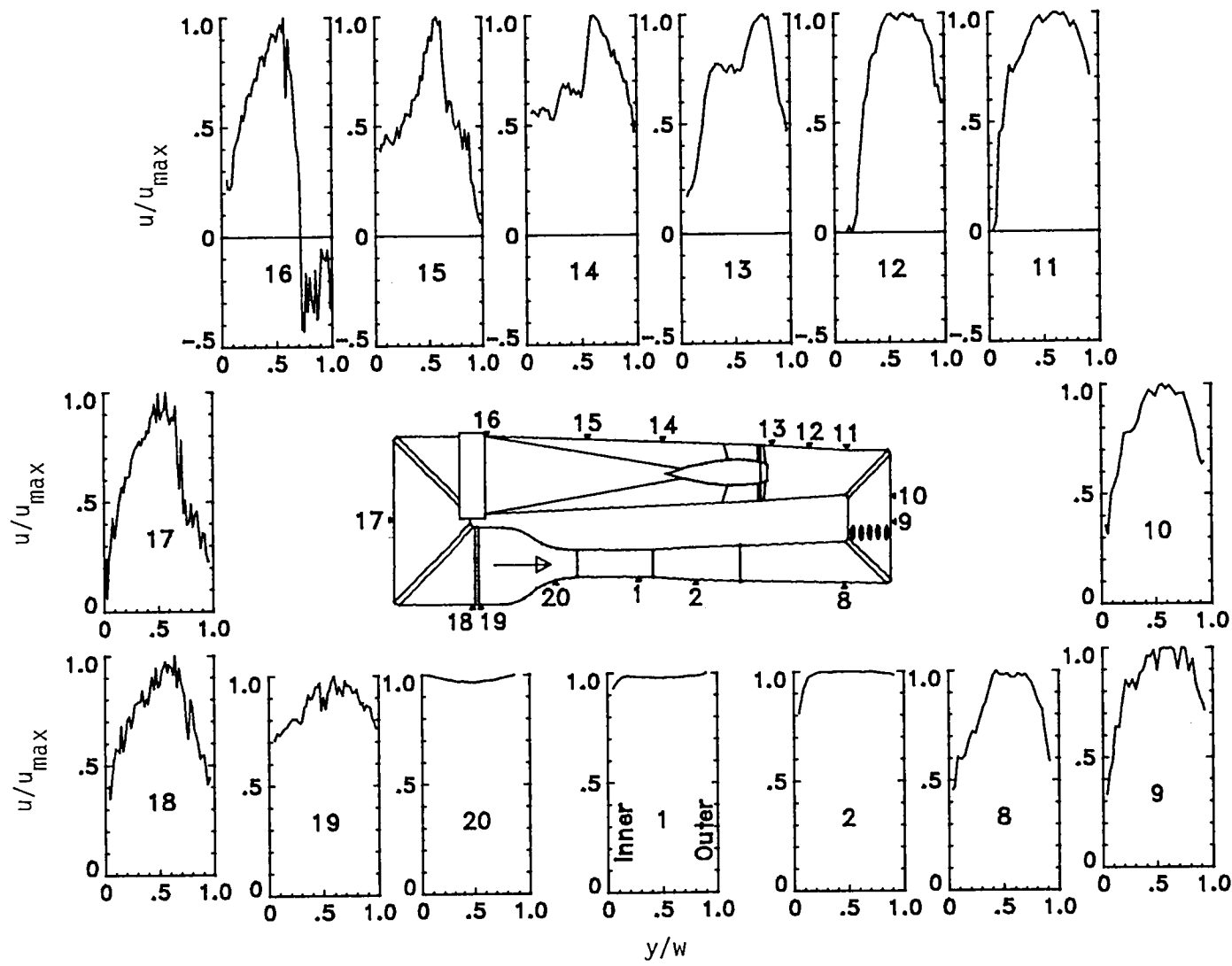


(n) Station 19. $w = 17.4$ m (57.0 ft).



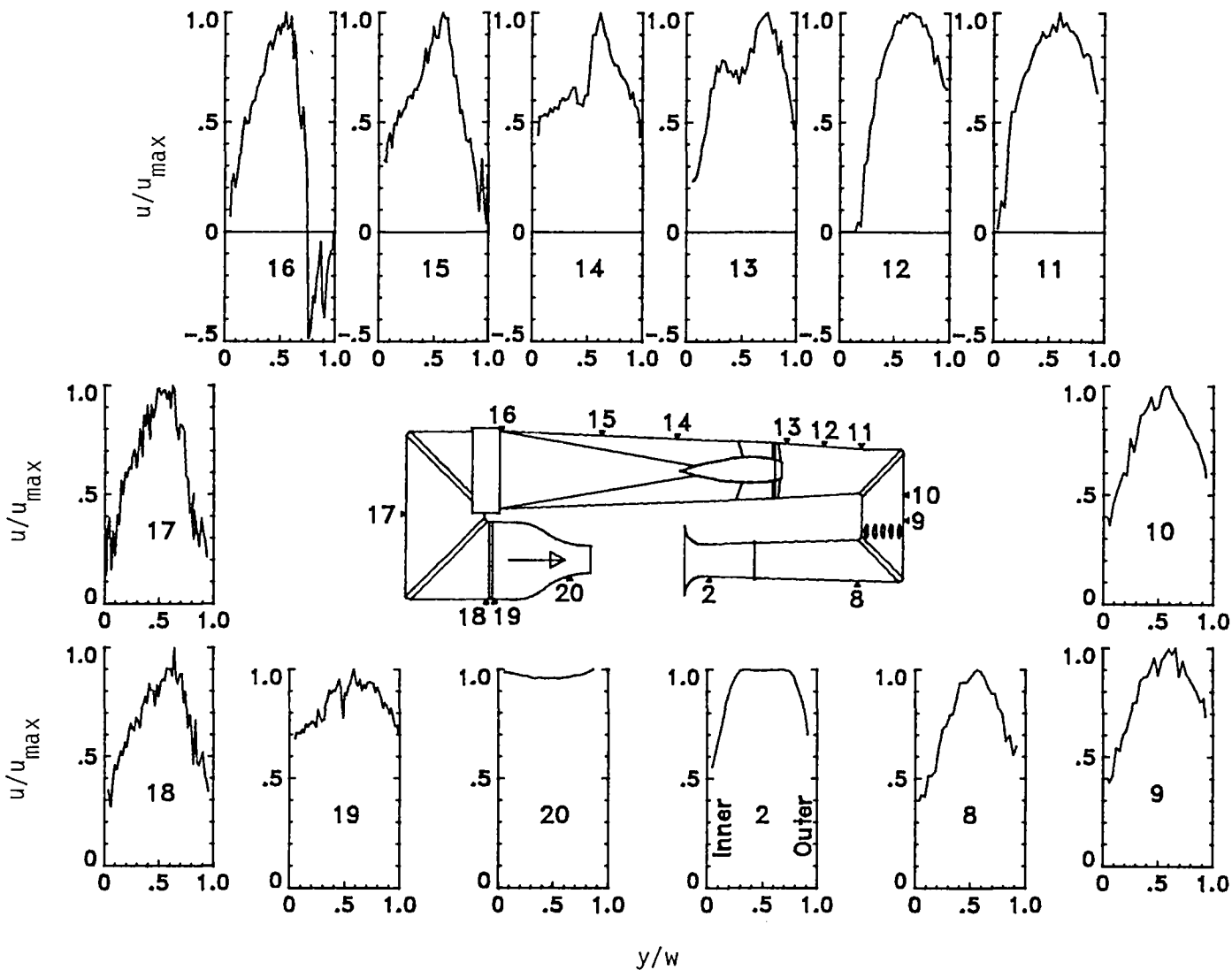
(o) Station 20. $w = 7.6$ m (24.9 ft).

Figure 7.- Concluded.



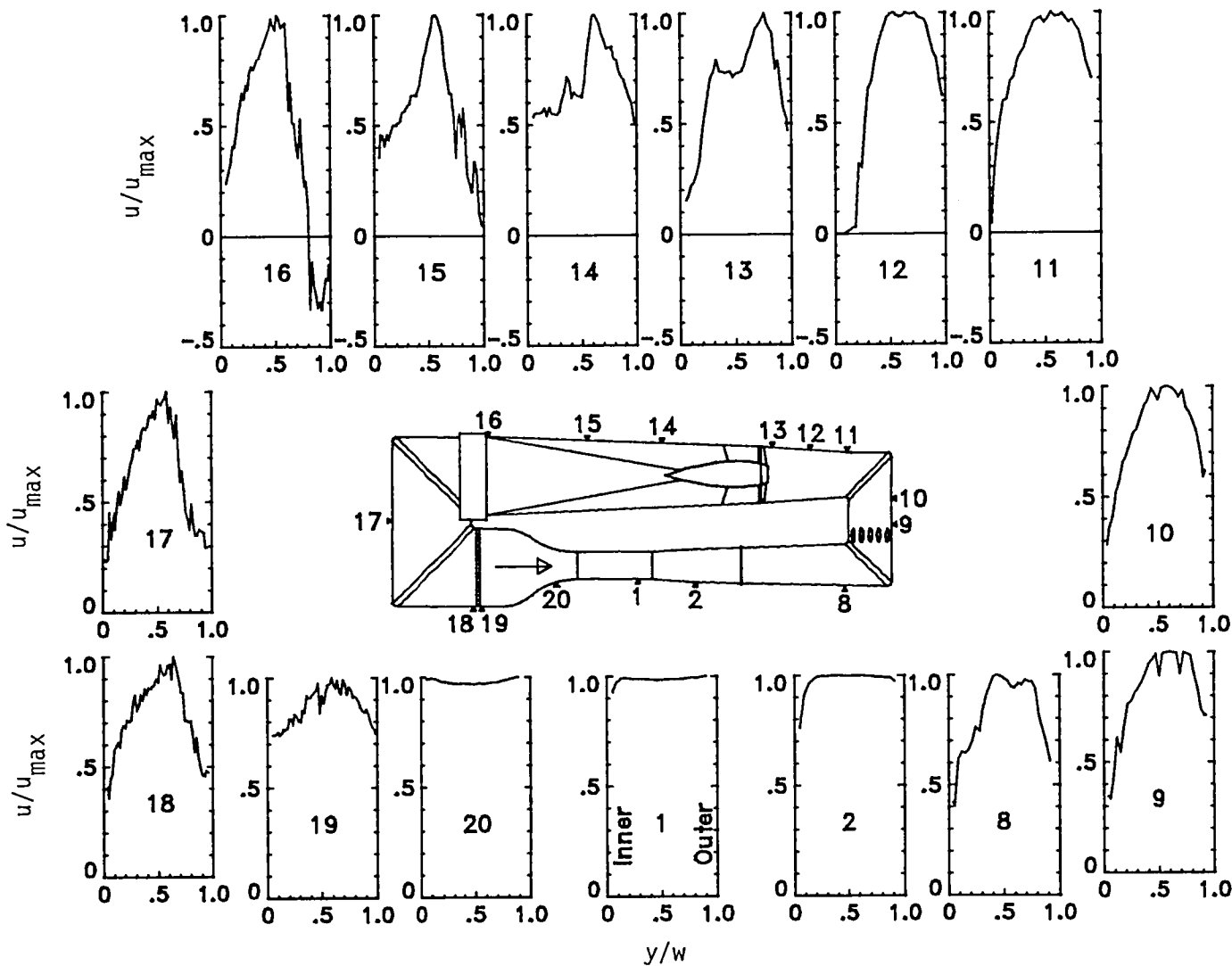
(a) Closed test section.

Figure 8.- Composite horizontal velocity profiles at $q_{TS} = 1.53 \text{ kPa}$ (32 psf).



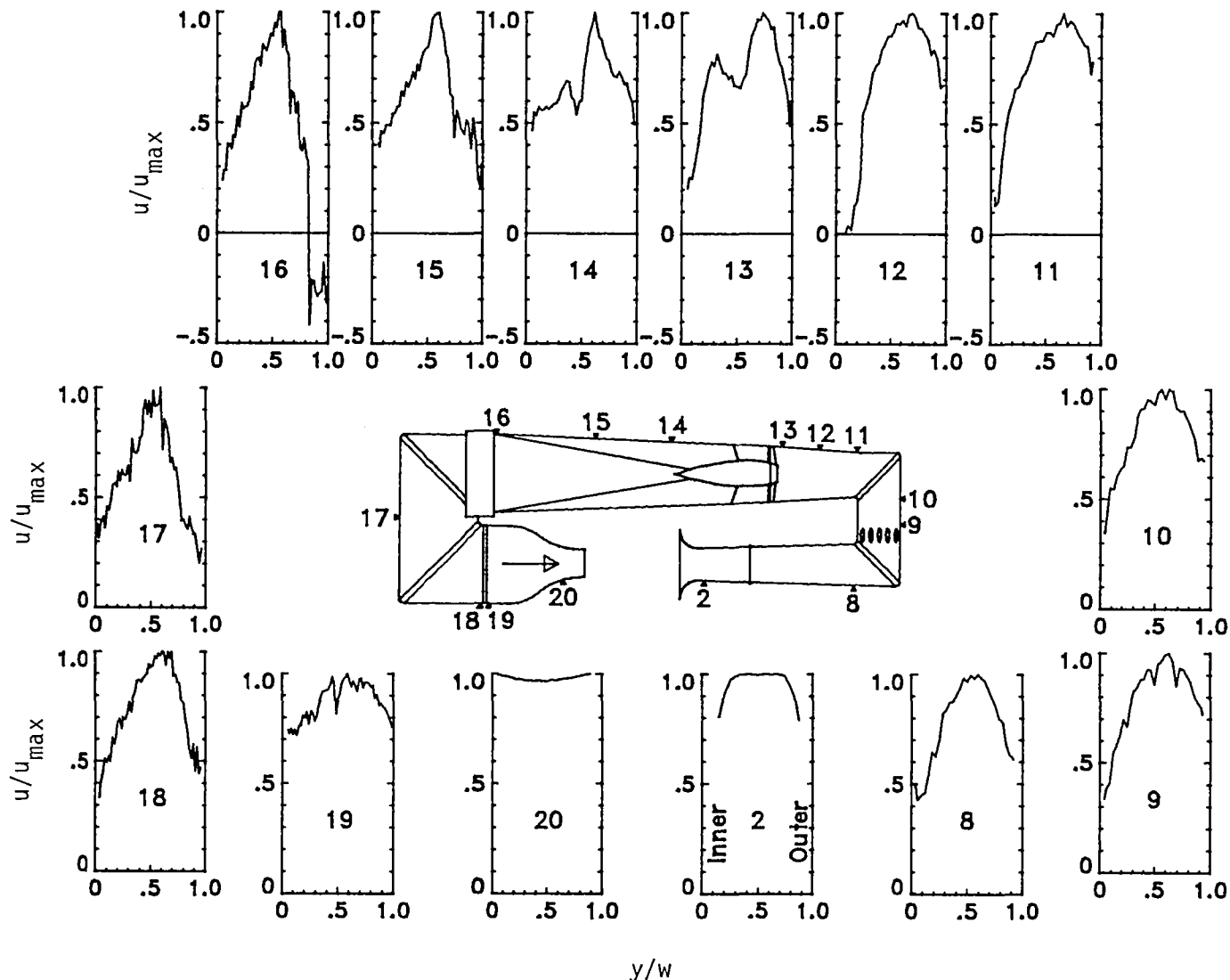
(b) Open test section.

Figure 8.- Concluded.



(a) Closed test section.

Figure 9.- Composite horizontal velocity profiles at $q_{TS} = 2.78 \text{ kPa}$ (58 psf).



(b) Open test section.

Figure 9.- Concluded.

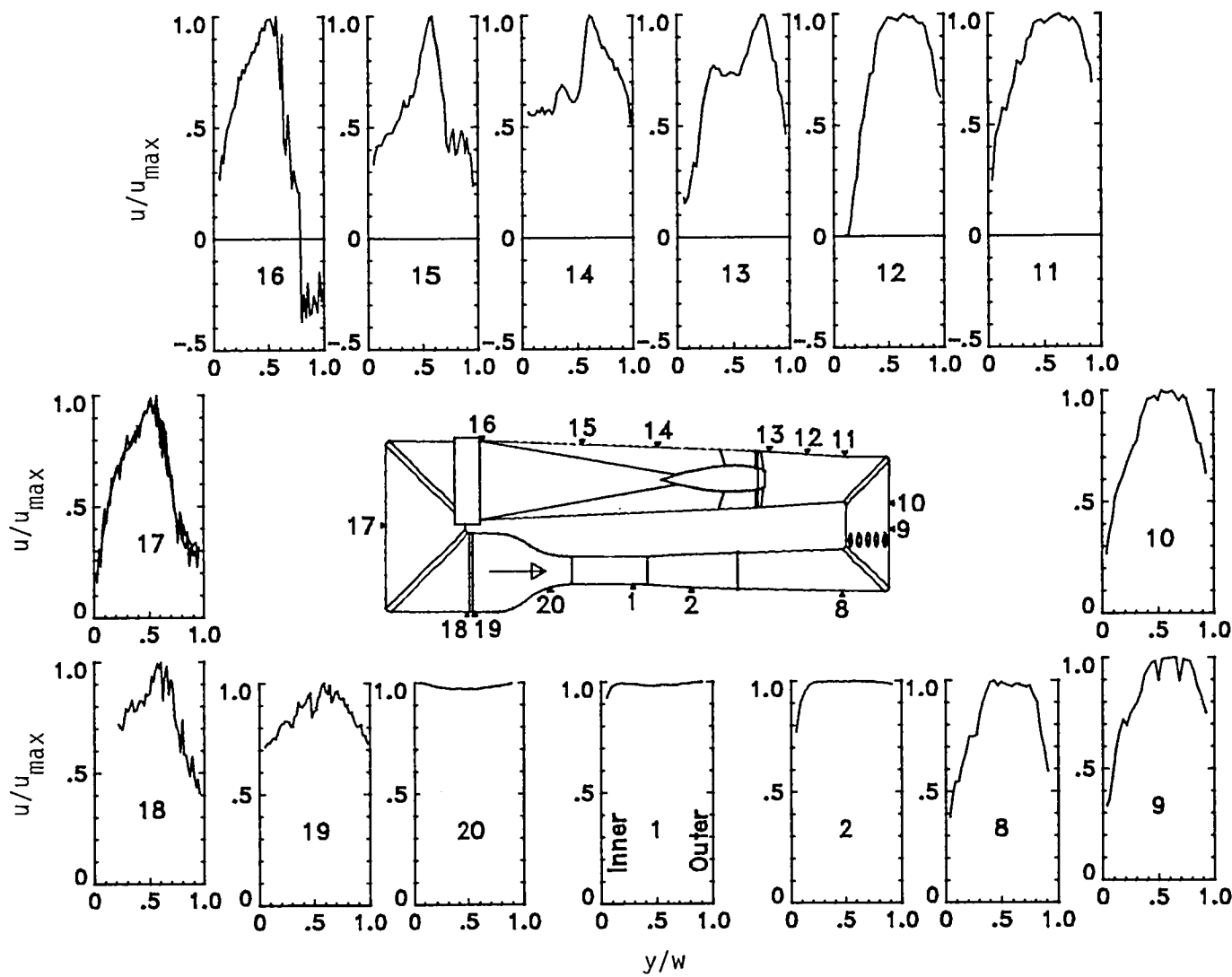
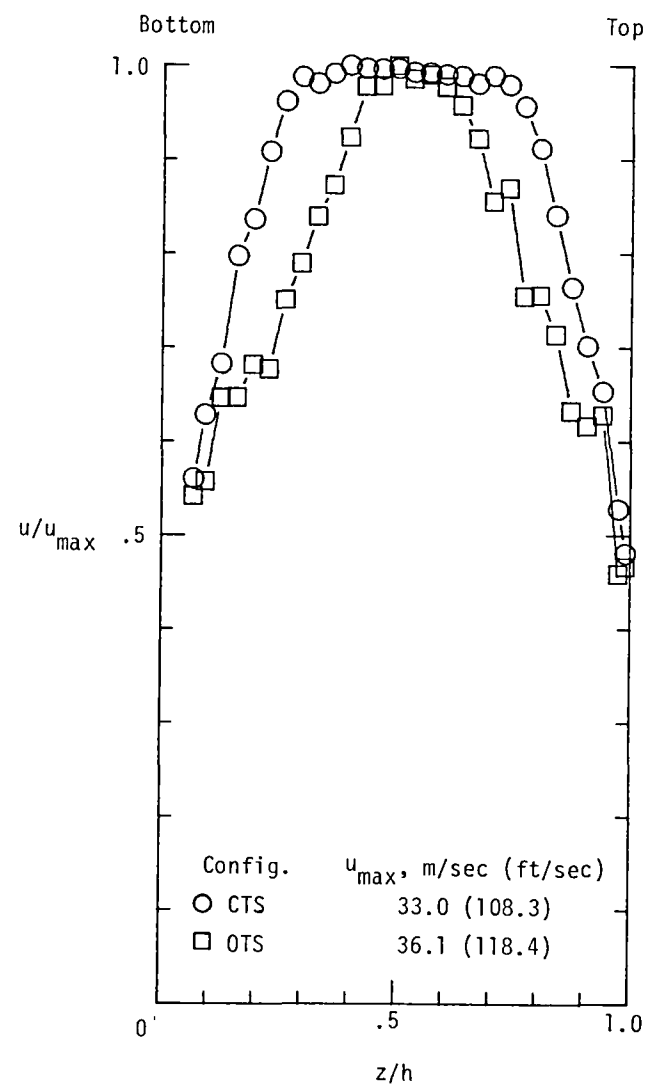
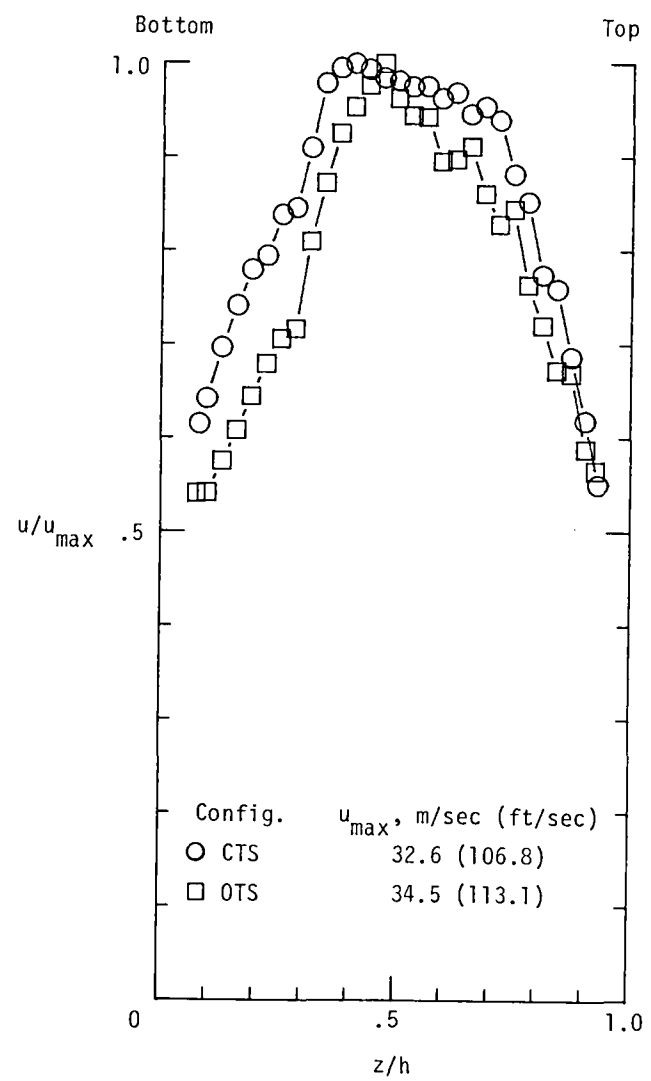


Figure 10.- Composite horizontal velocity profiles at $q_{TS} = 4.79$ kPa (100 psf) for closed test section.



(a) Station 10. $h = 9.0$ m (29.5 ft).



(b) Station 11. $h = 9.8$ m (32.3 ft).

Figure 11.- Vertical velocity profiles at $q_{TS} = 2.78$ kPa (58 psf).

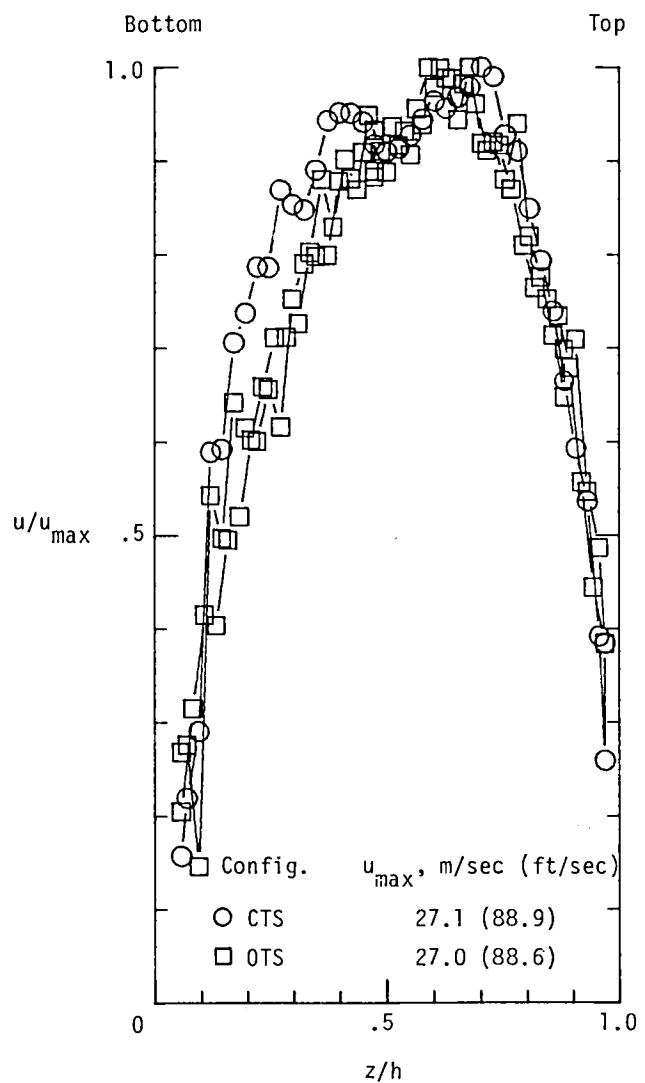
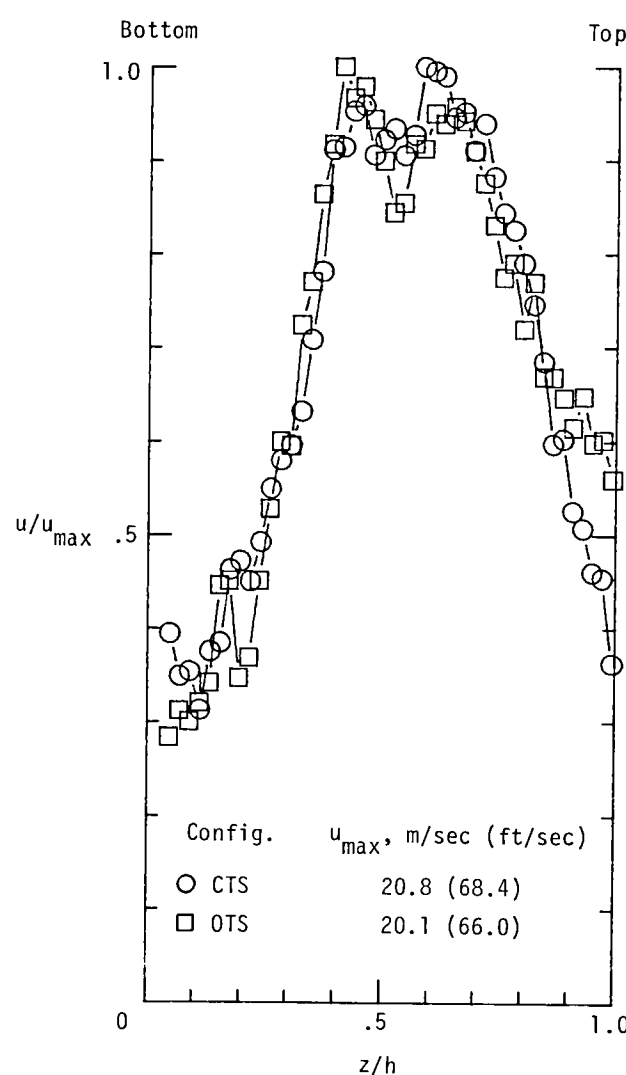
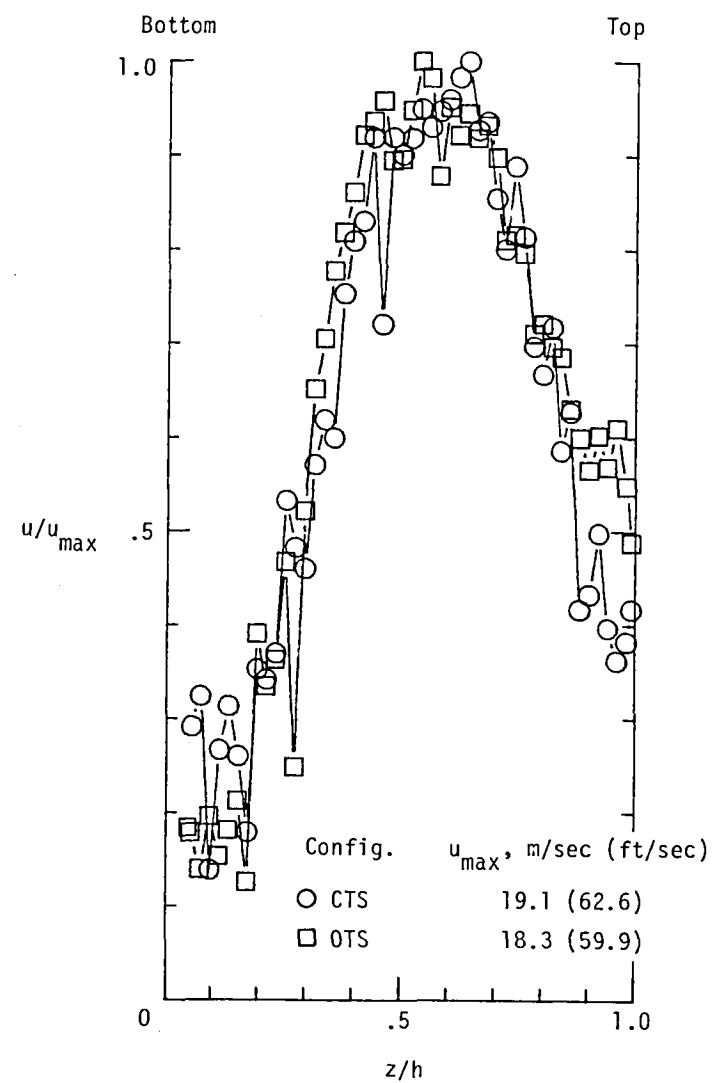
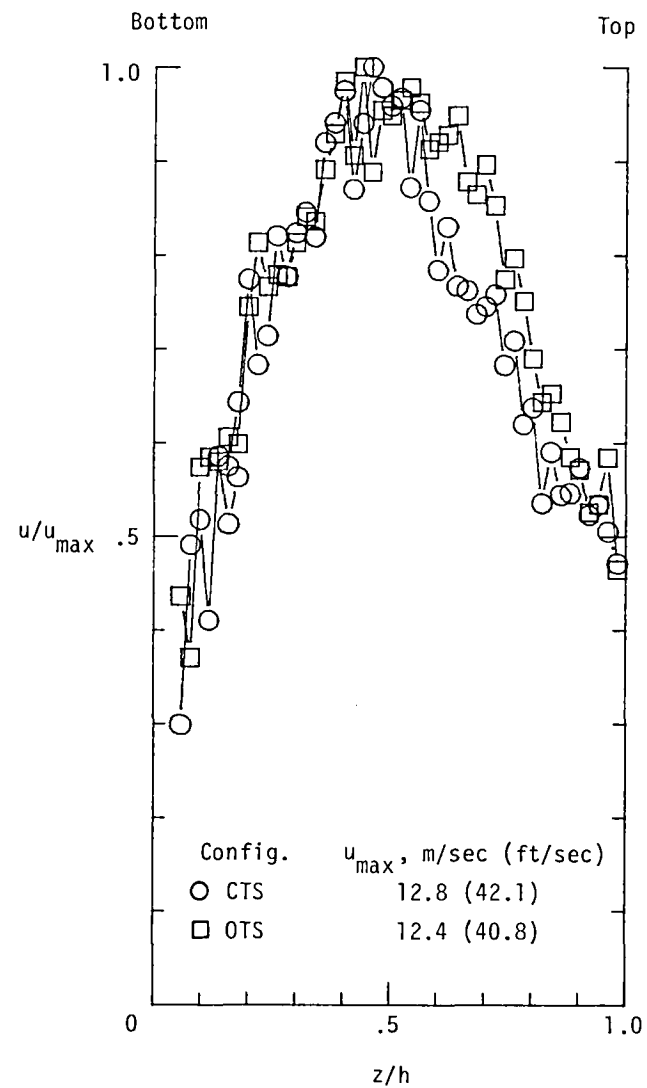
(c) Station 13. $h = 12.0$ m (39.5 ft).(d) Station 15. $h = 14.2$ m (46.5 ft).

Figure 11.- Continued.



(e) Station 16. $h = 15.2$ m (49.8 ft).



(f) Station 18-1. $h = 15.2$ m (49.8 ft).

Figure 11.—Continued.

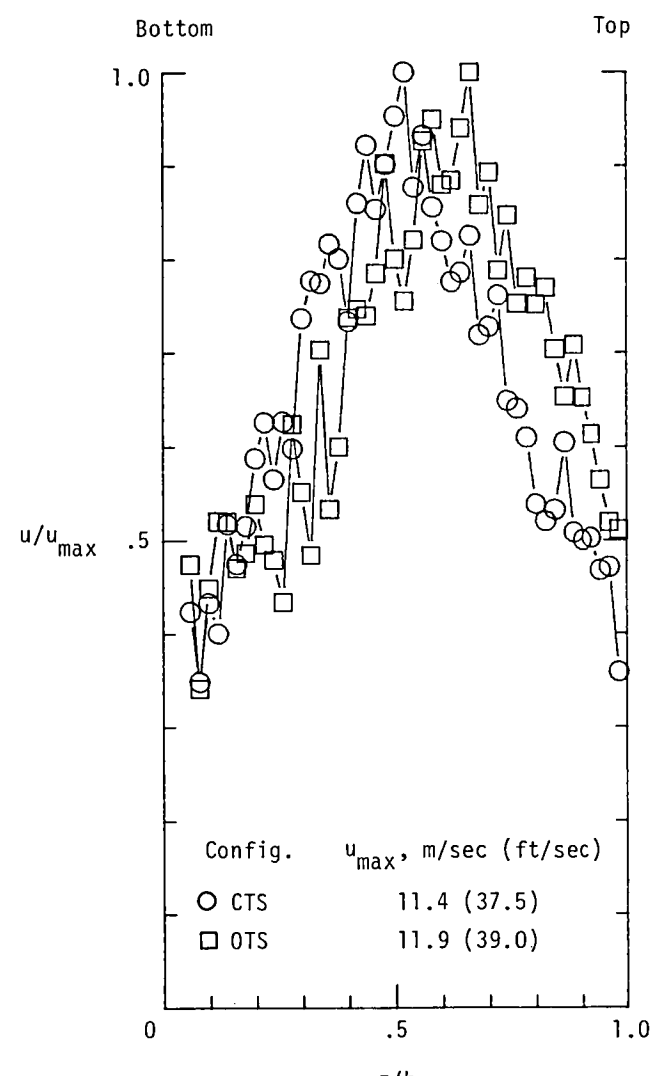
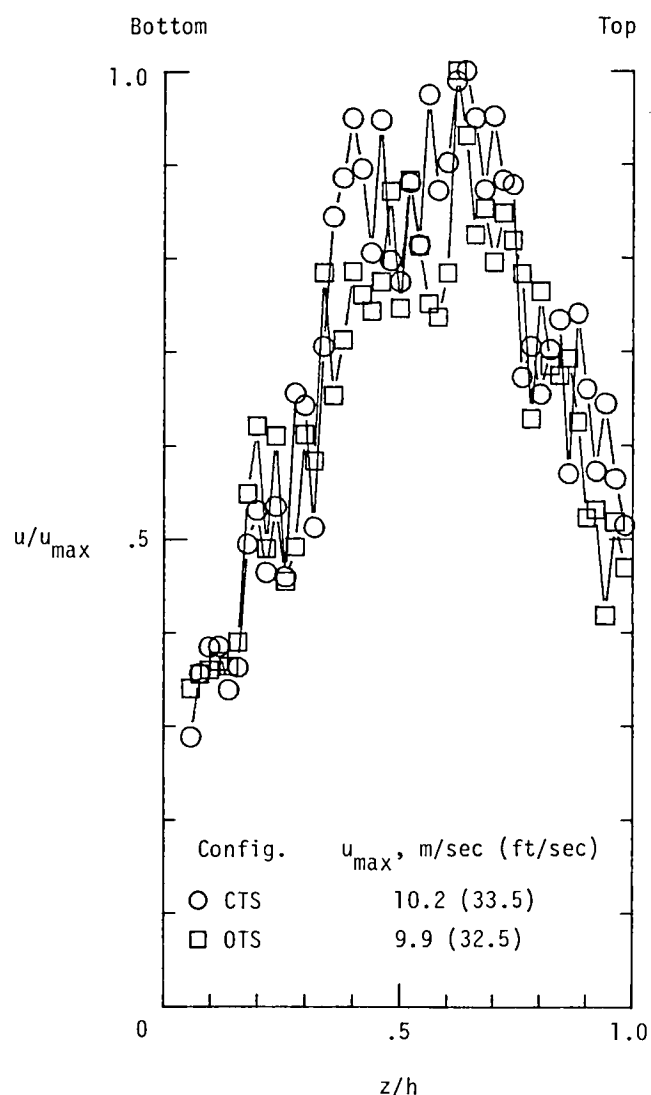
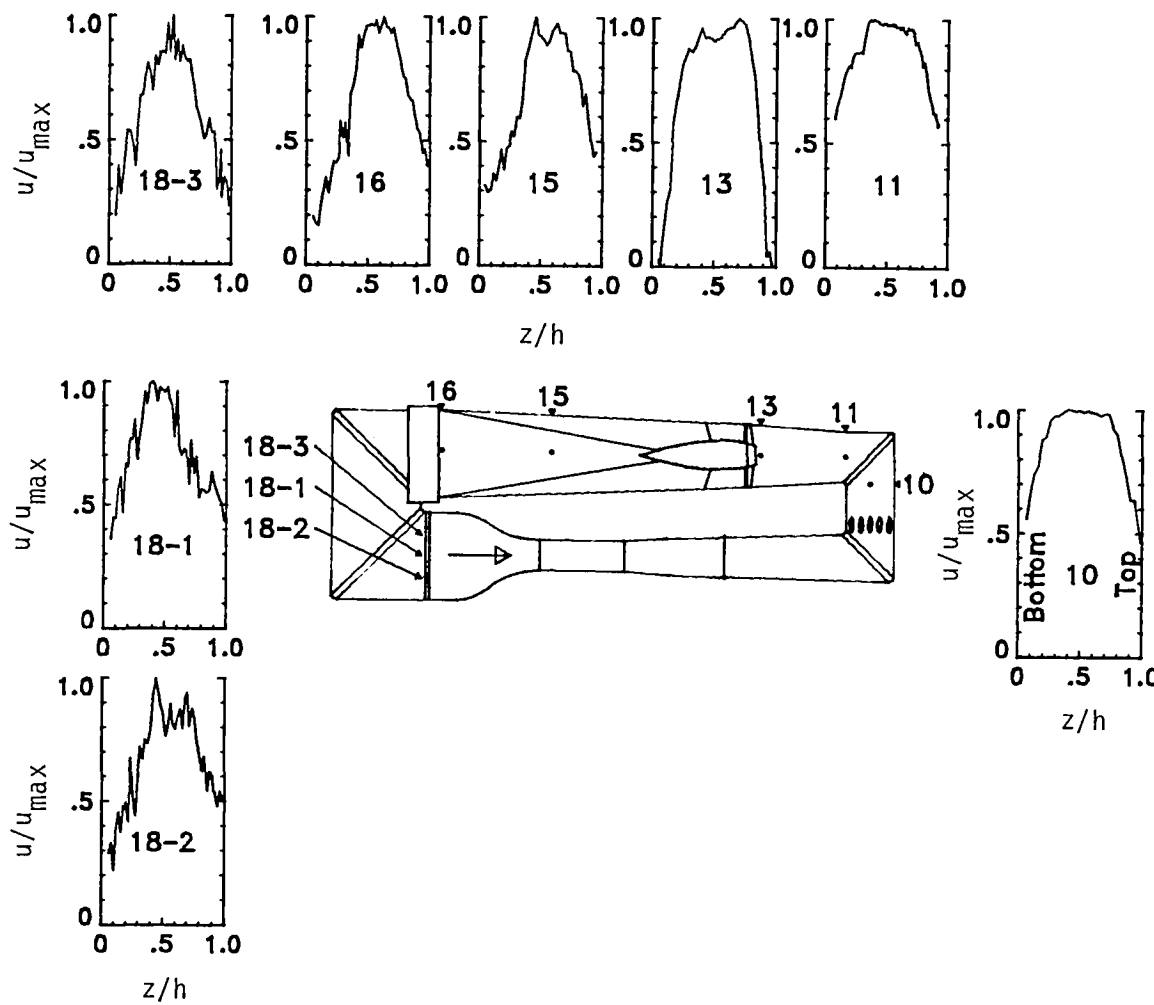
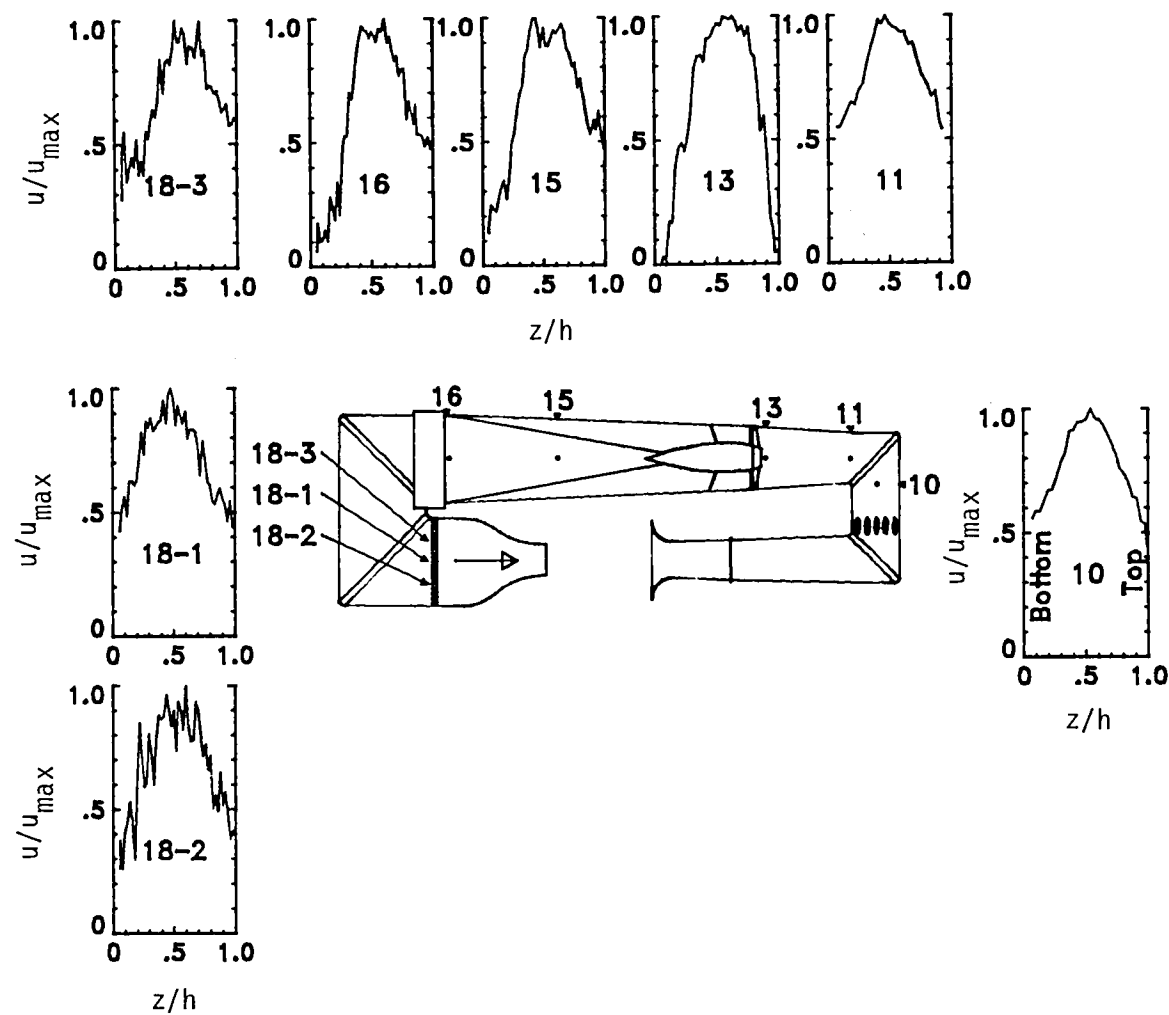
(g) Station 18-2. $h = 15.2$ m (49.8 ft).(h) Station 18-3. $h = 15.2$ m (49.8 ft).

Figure 11.- Concluded.



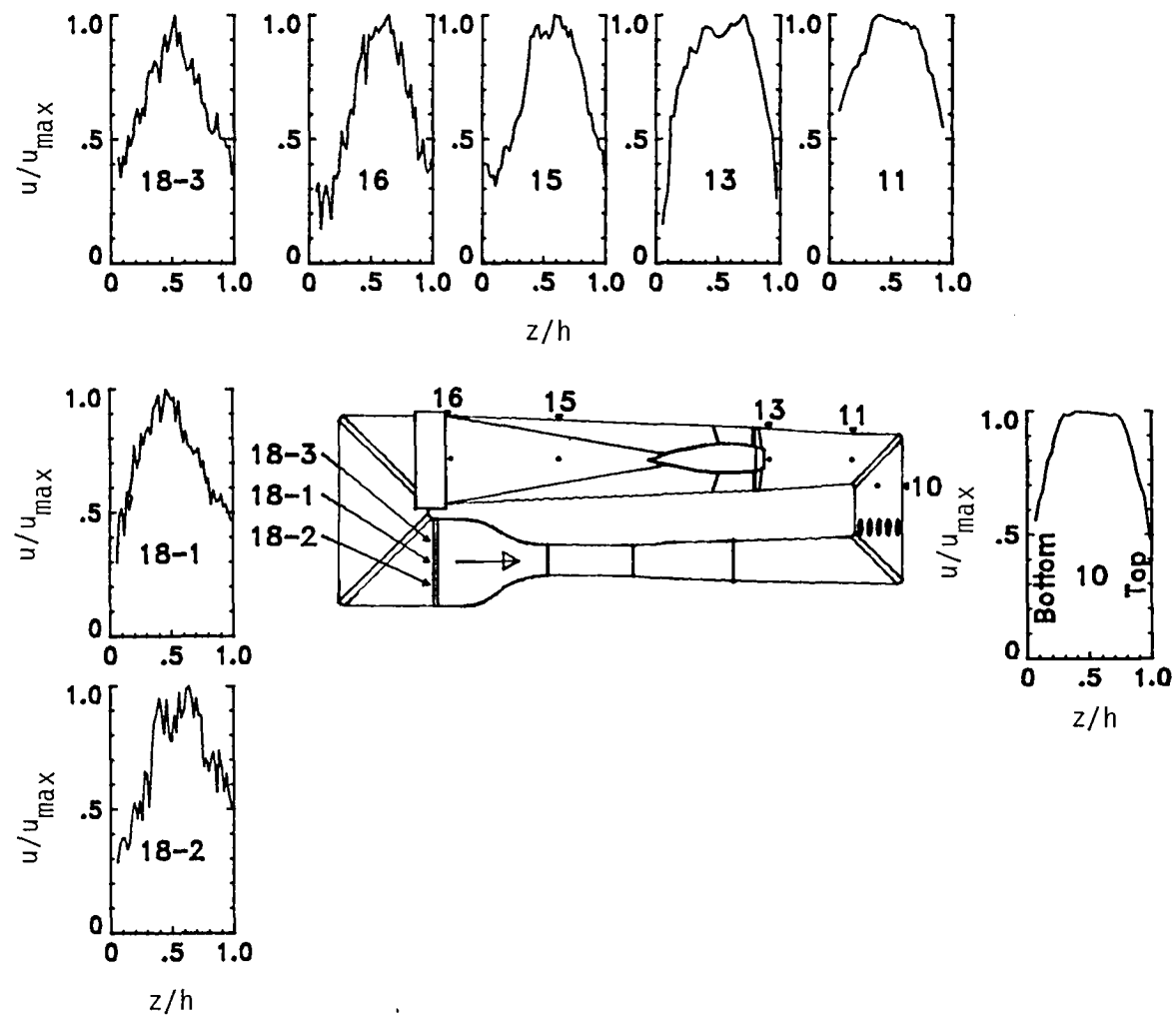
(a) Closed test section.

Figure 12.- Composite vertical velocity profiles at $q_{TS} = 1.53 \text{ kPa}$
 (32 psf) .



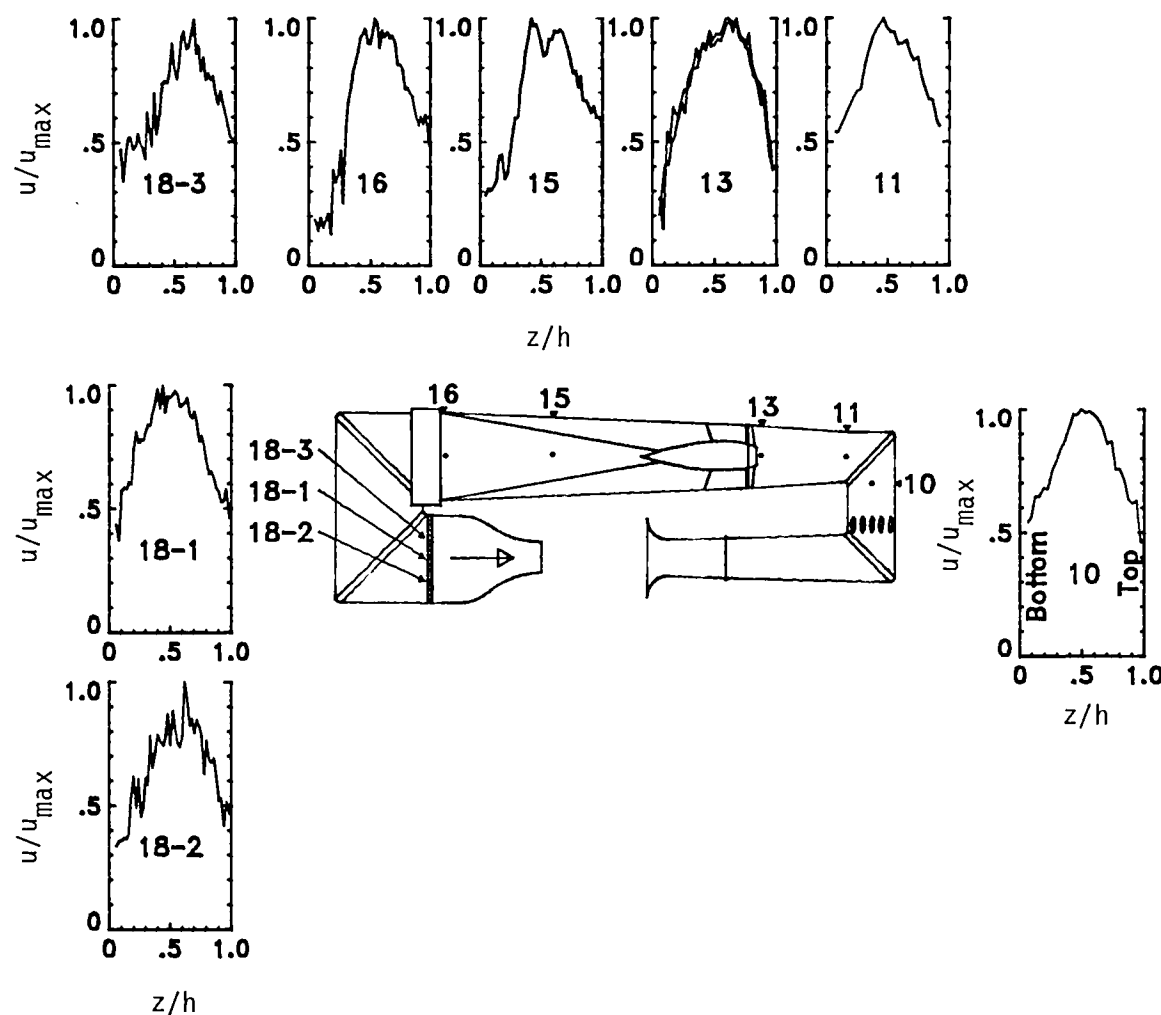
(b) Open test section.

Figure 12.- Concluded.



(a) Closed test section.

Figure 13.-- Composite vertical velocity profiles at $q_{TS} = 2.78 \text{ kPa}$
 (58 psf) .



(b) Open test section.

Figure 13.- Concluded.

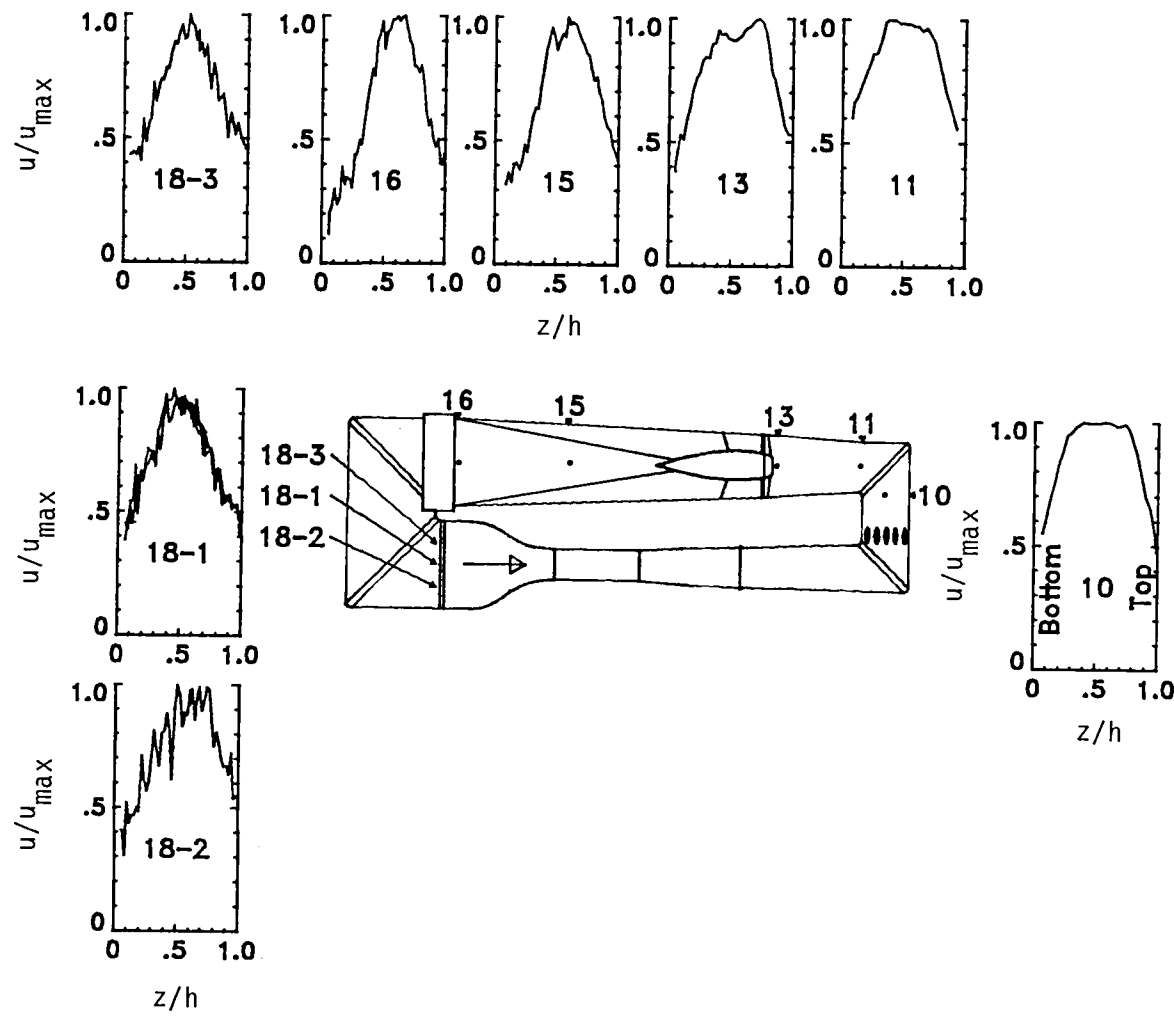
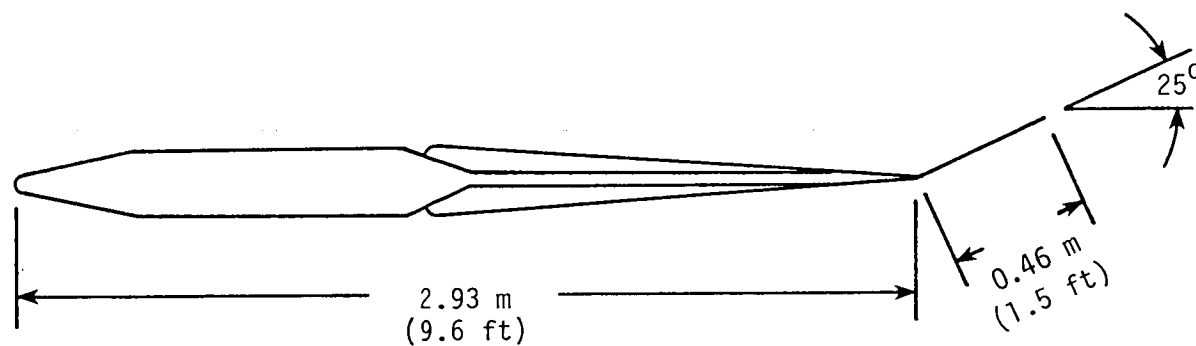


Figure 14.- Composite vertical velocity profiles at $q_{TS} = 4.79$ kPa
(100 psf) for closed test section.



(a) Cross-sectional view.

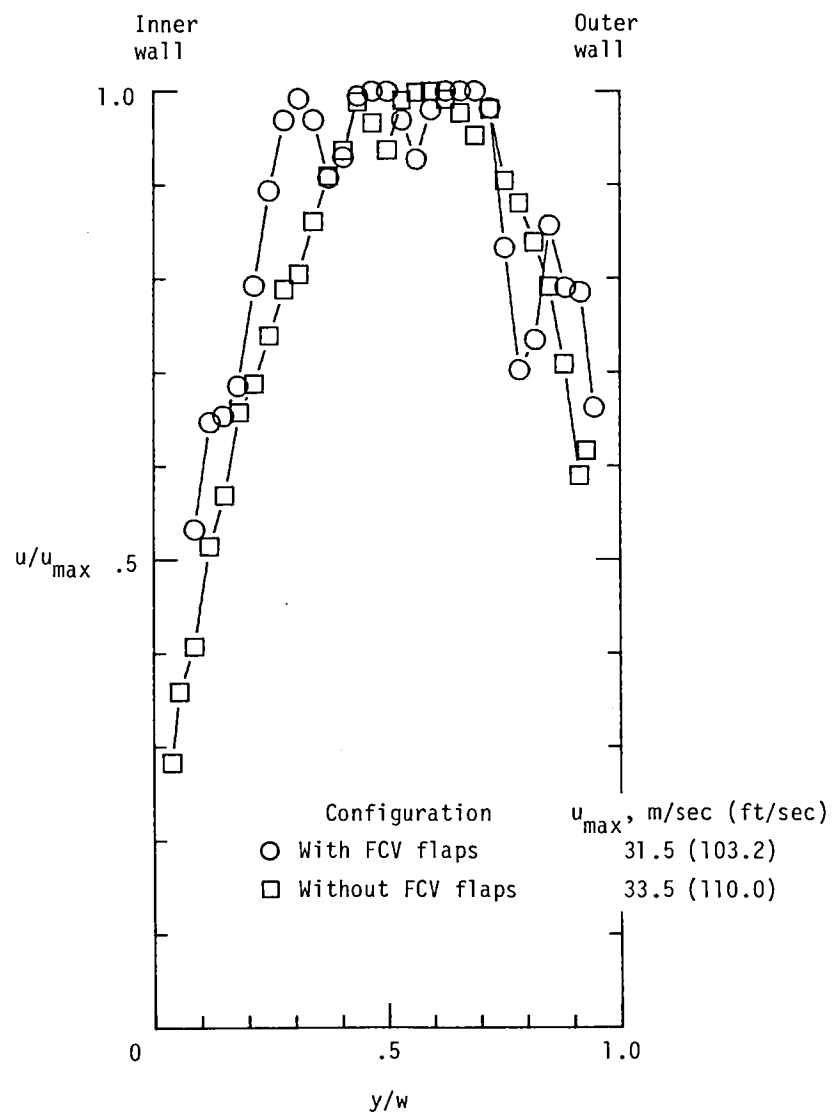
Figure 15.- Flow-control vane (FCV) with trailing-edge flap (flow deflector) installed.



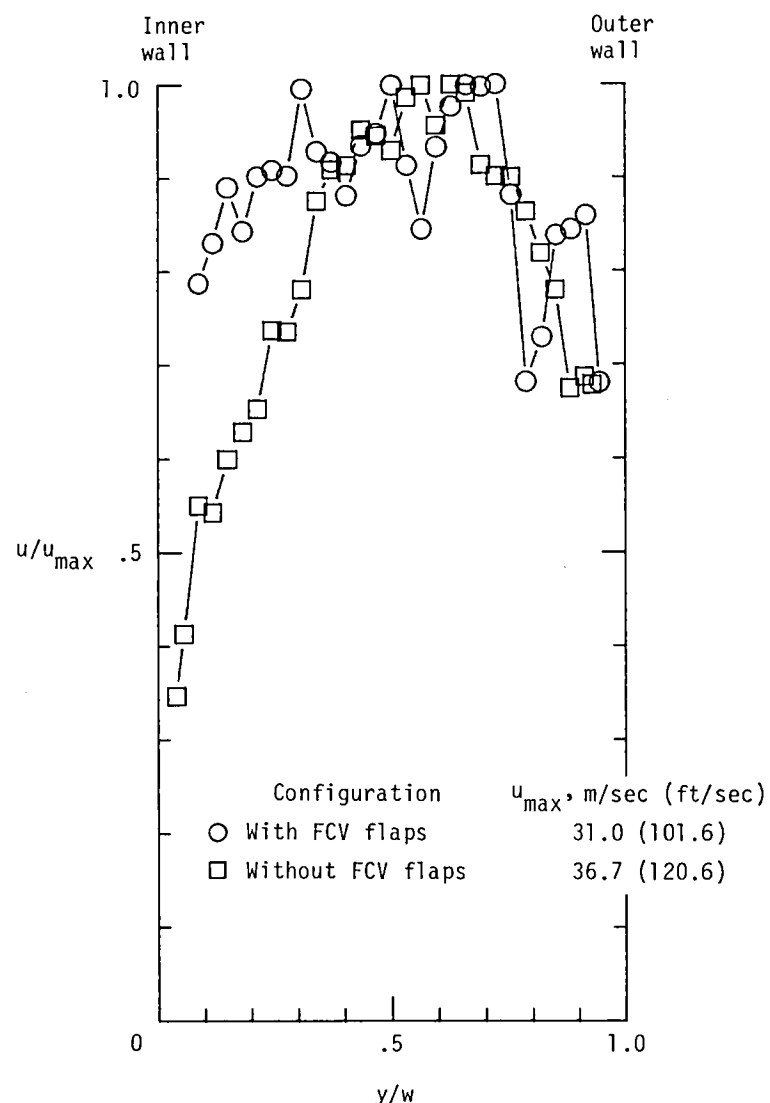
L-83-8075

(b) Rear view.

Figure 15.- Concluded.

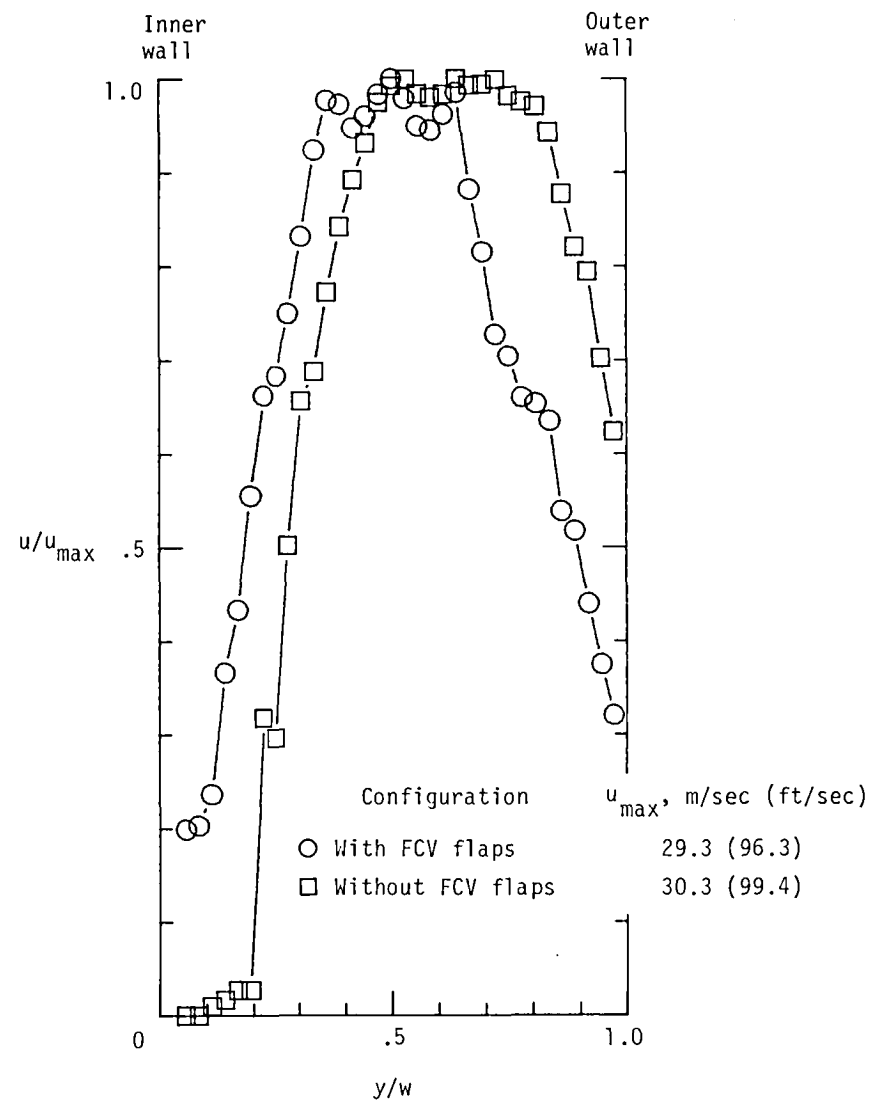


(a) Station 10. Closed test section.

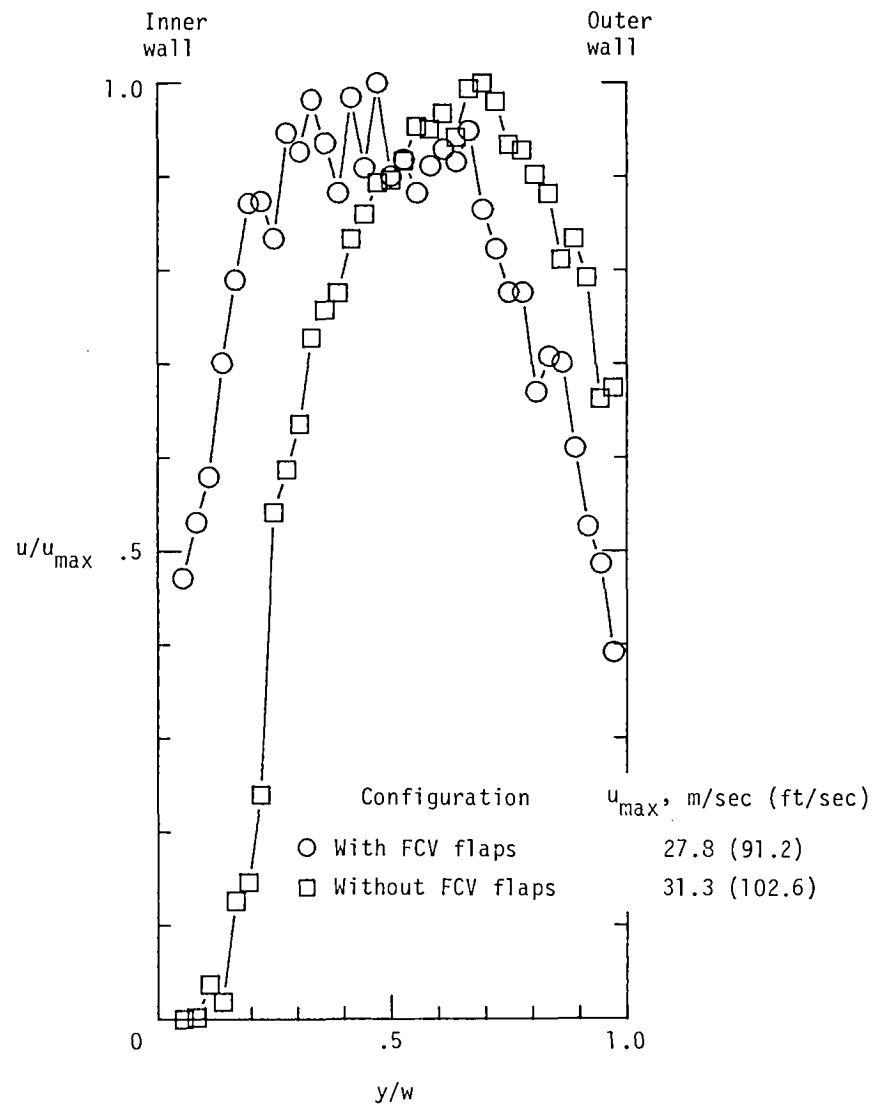


(b) Station 10. Open test section.

Figure 16.- Effect of FCV trailing-edge flaps on horizontal velocity profiles at $q_{TS} = 2.78 \text{ kPa } (58 \text{ psf})$.

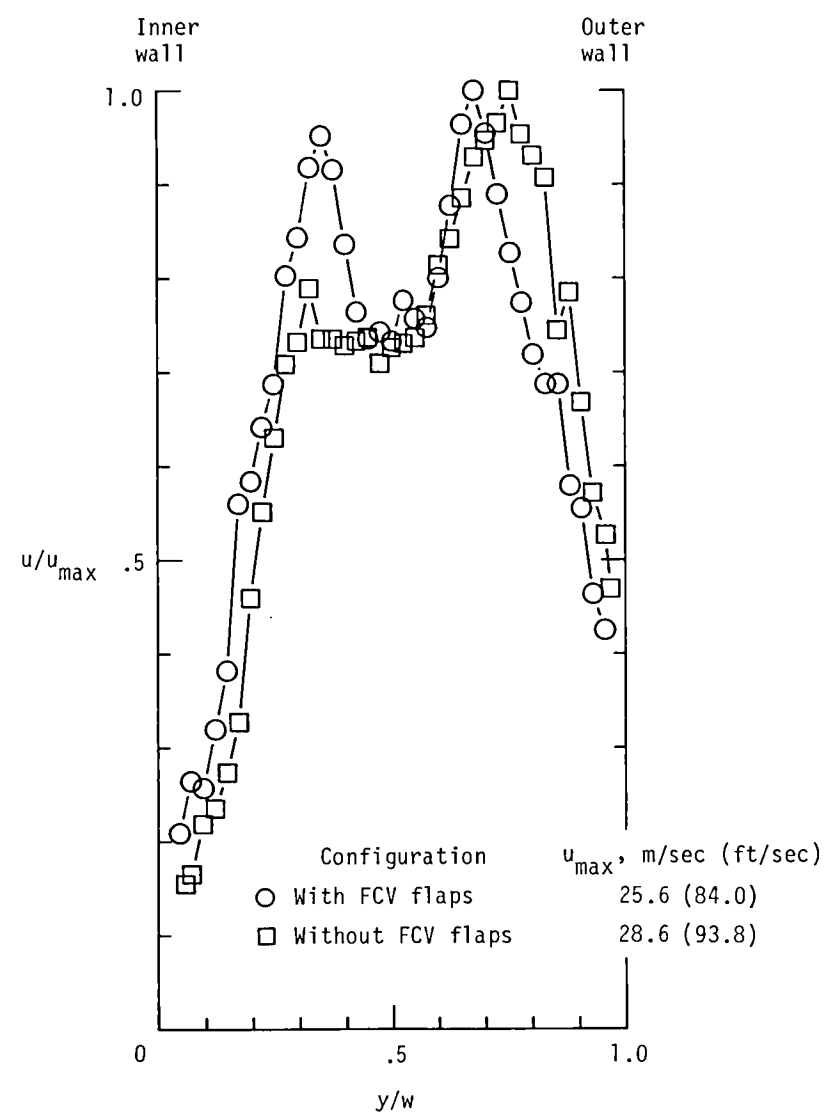


(c) Station 12. Closed test section.

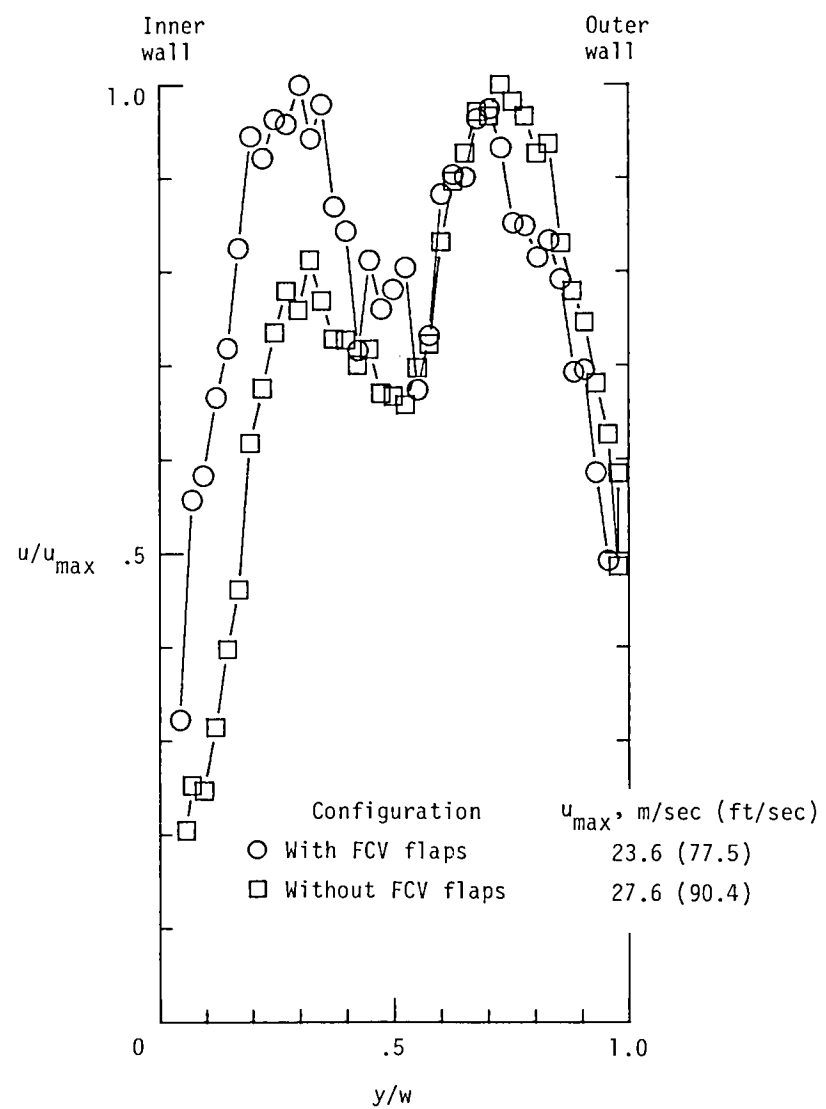


(d) Station 12. Open test section.

Figure 16.- Continued.

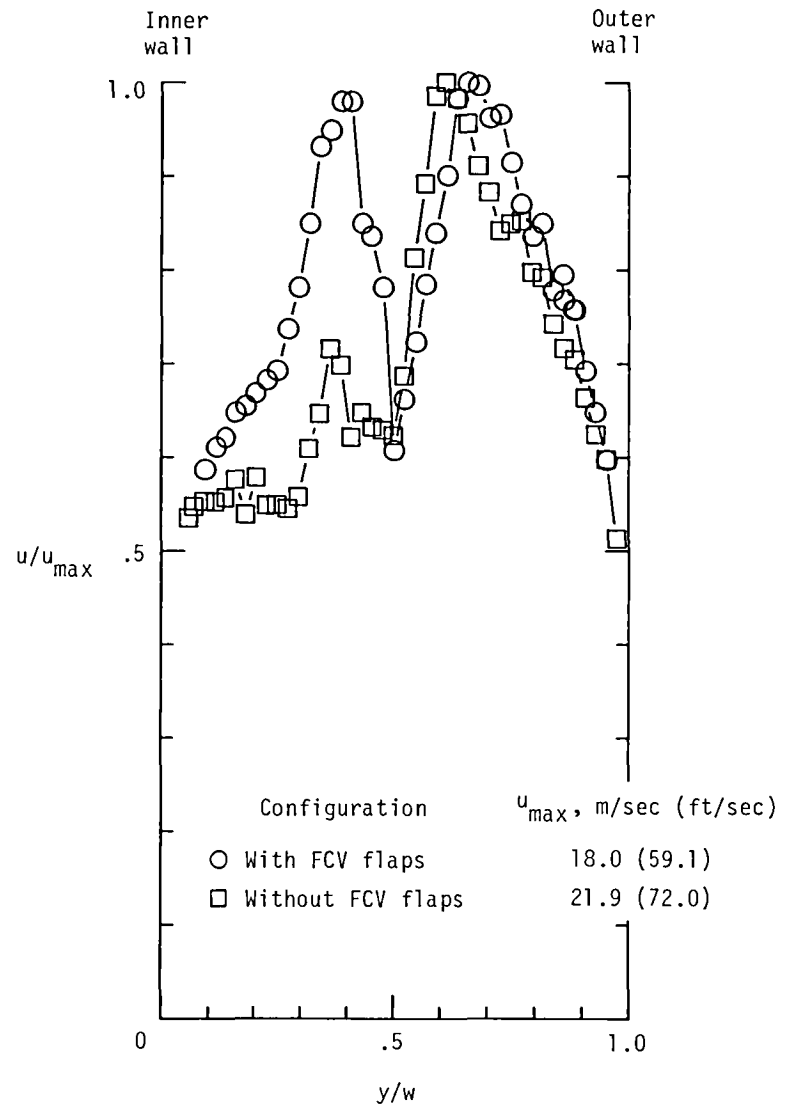


(e) Station 13. Closed test section.

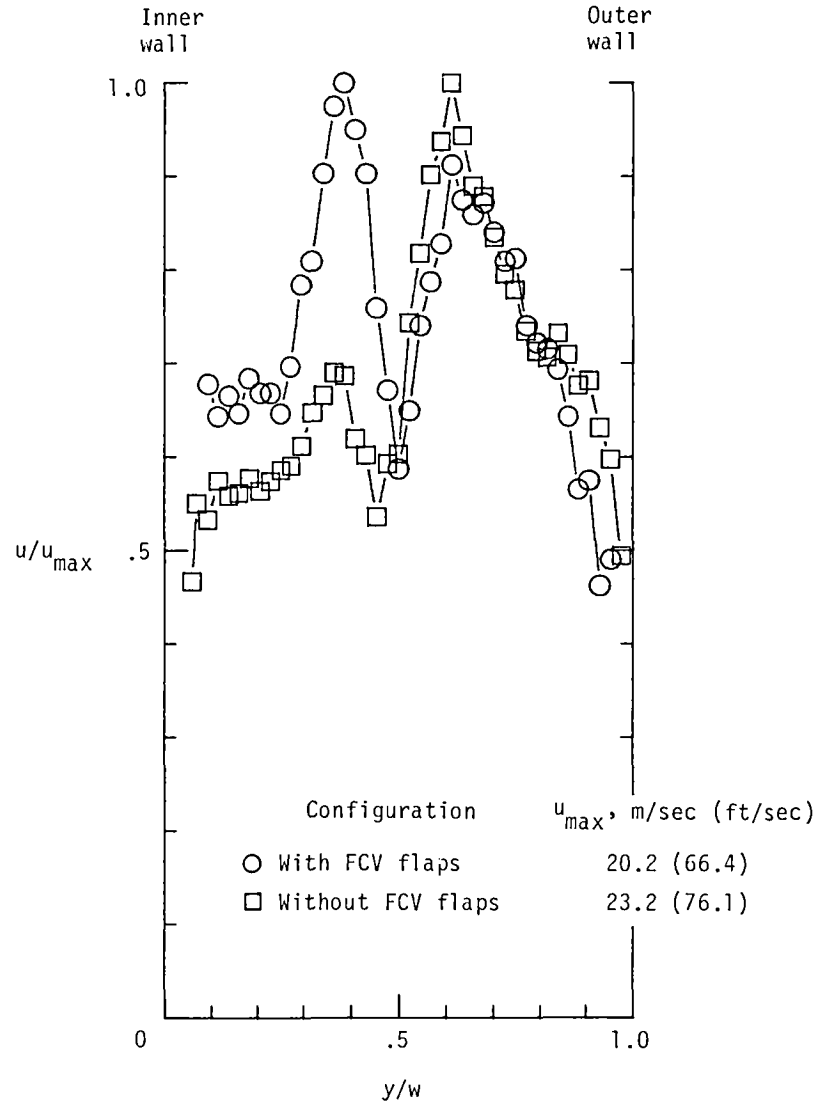


(f) Station 13. Open test section.

Figure 16.- Continued.

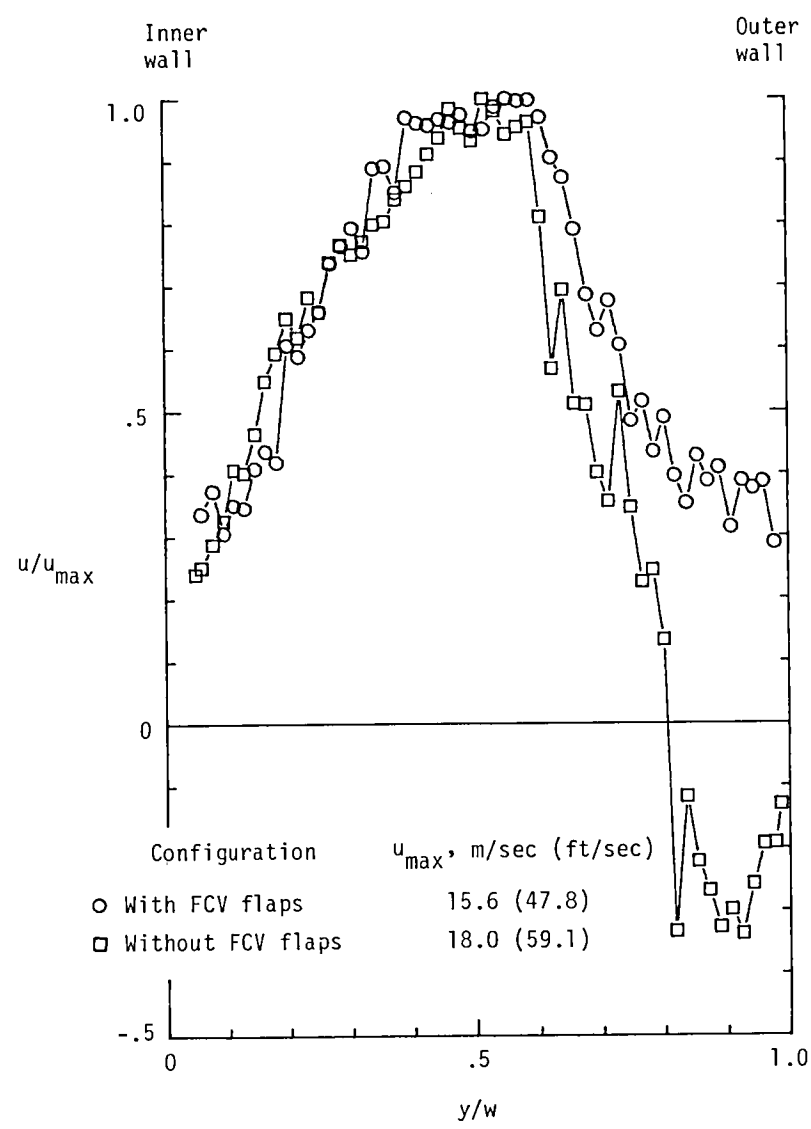


(g) Station 14. Closed test section.



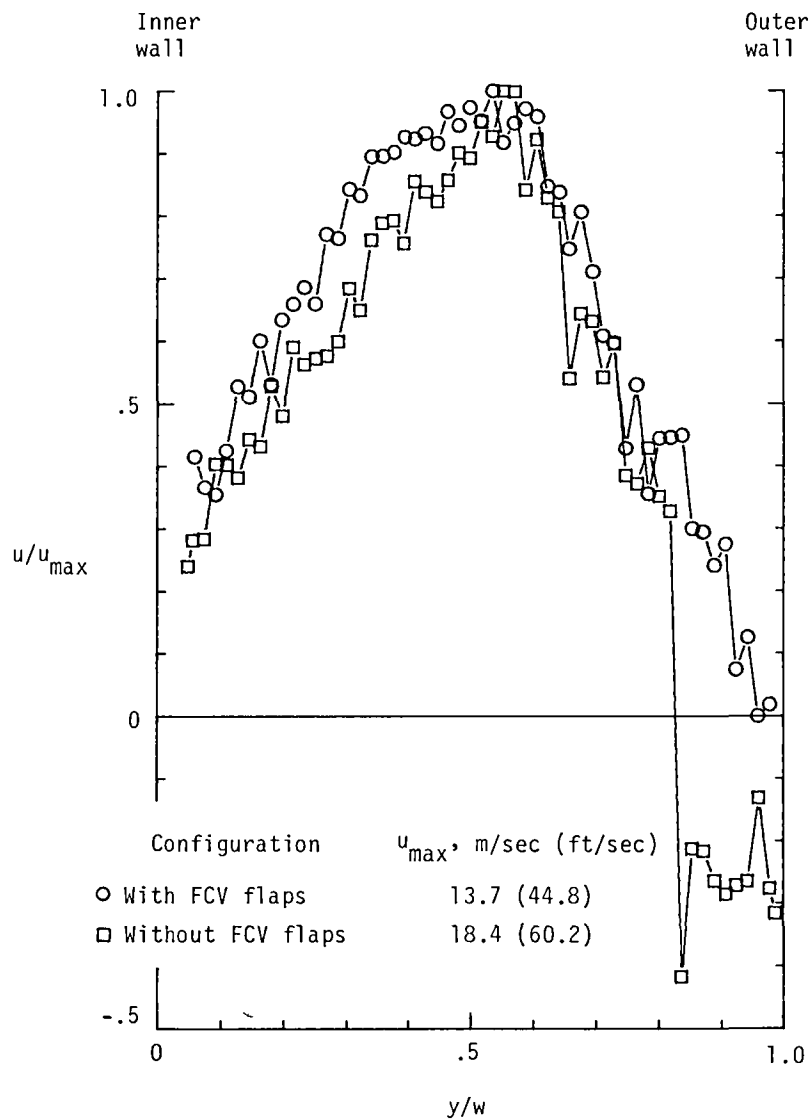
(h) Station 14. Open test section.

Figure 16.- Continued.



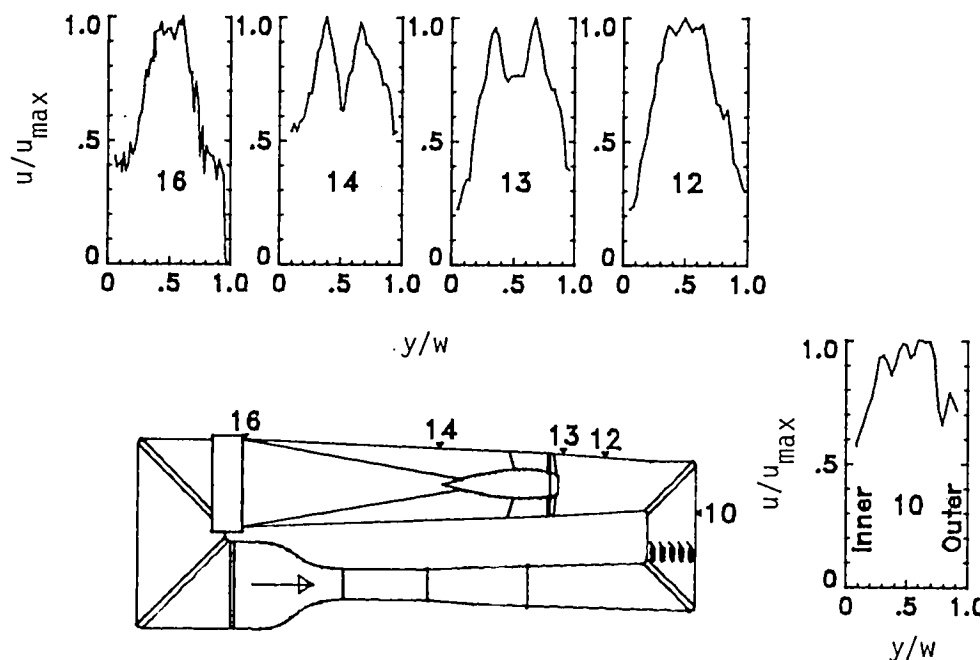
(i) Station 16. Closed test section.

Figure 16.- Continued.



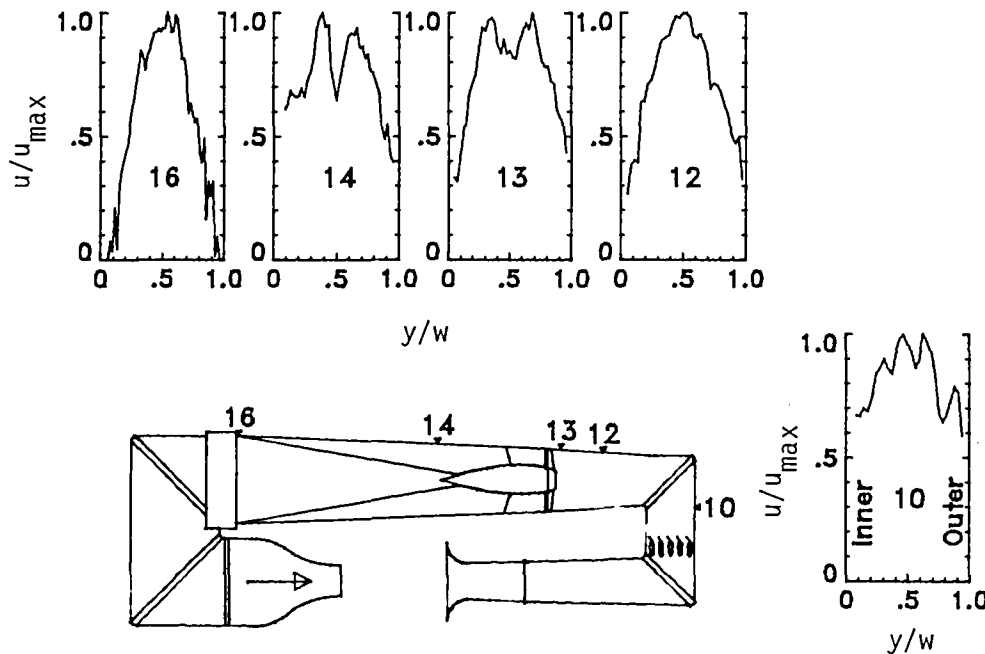
(j) Station 16.- Open test section.

Figure 16.- Concluded.



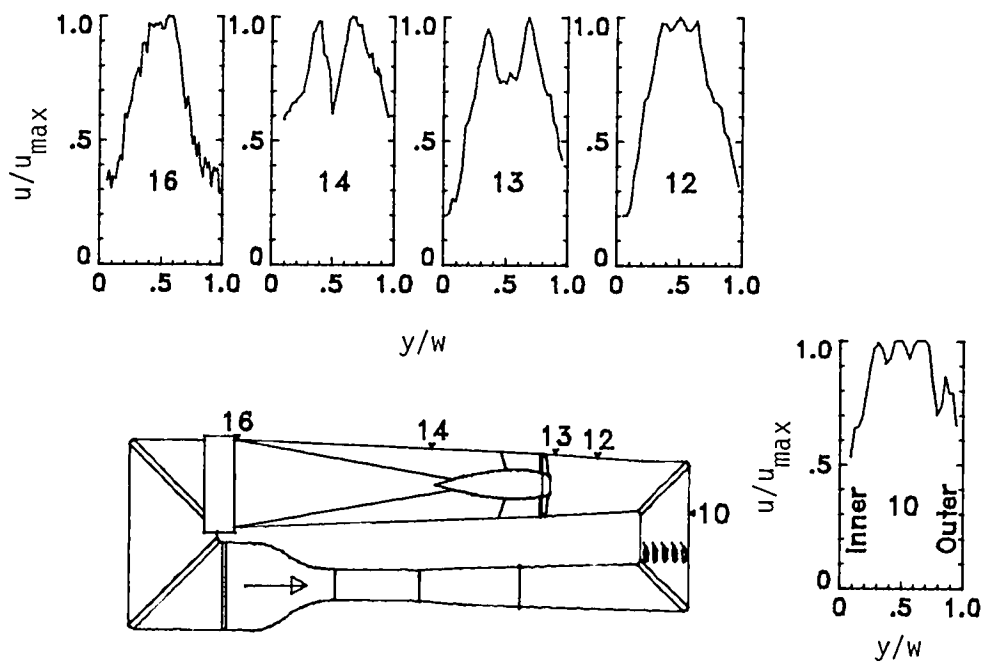
(a) Closed test section.

Figure 17.- Composite horizontal velocity profiles with trailing-edge flaps on flow-control vanes at $q_{TS} = 1.53 \text{ kPa}$ (32 psf).



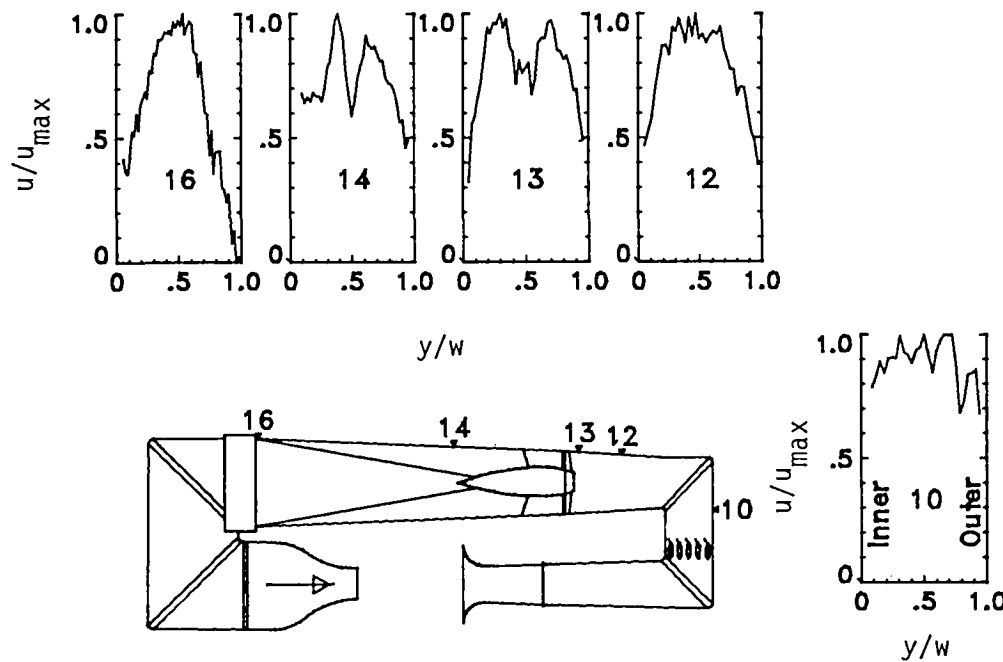
(b) Open test section.

Figure 17.- Concluded.



(a) Closed test section.

Figure 18.- Composite horizontal velocity profiles with trailing-edge flaps on flow-control vanes at $q_{TS} = 2.78 \text{ kPa}$ (58 psf).



(b) Open test section.

Figure 18.- Concluded.

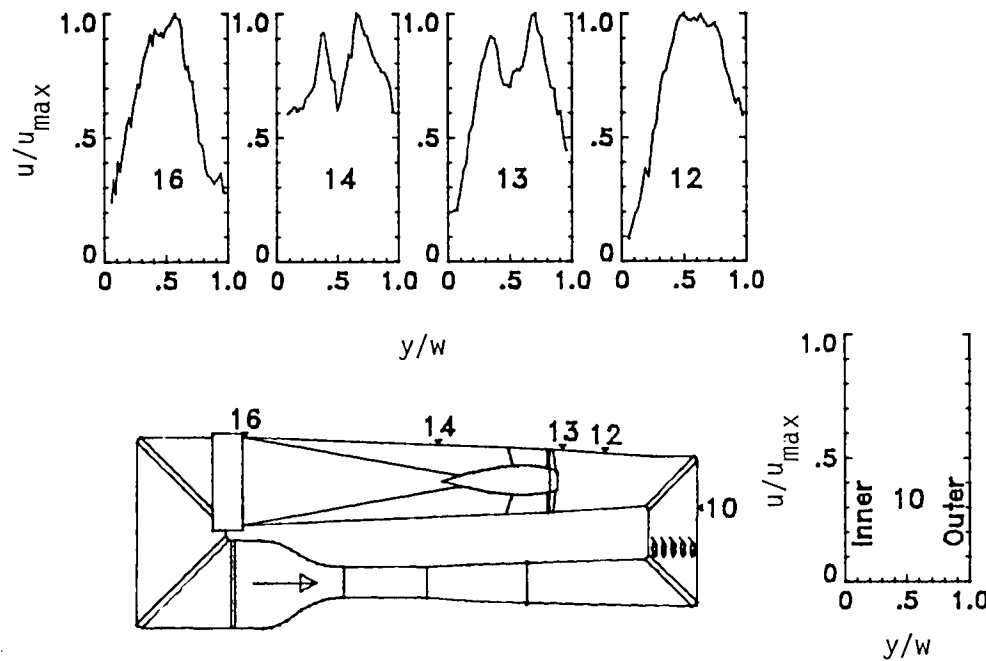


Figure 19.- Composite horizontal velocity profiles with trailing-edge flaps on flow-control vanes at $q_{\text{TS}} = 4.79 \text{ kPa}$ (100 psf) for closed test section.

1. Report No. NASA TM-85662	2. Government Accession No.	3. Recipient's Catalog No.	
4. Title and Subtitle FLOW IMPROVEMENTS IN THE CIRCUIT OF THE LANGLEY 4- BY 7-METER TUNNEL		5. Report Date December 1983	
7. Author(s) Zachary T. Applin		6. Performing Organization Code 505-42-23-09	
9. Performing Organization Name and Address NASA Langley Research Center Hampton, VA 23665		8. Performing Organization Report No. L-15631	
12. Sponsoring Agency Name and Address National Aeronautics and Space Administration Washington, DC 20546		10. Work Unit No.	
		11. Contract or Grant No.	
		13. Type of Report and Period Covered Technical Memorandum	
		14. Sponsoring Agency Code	
15. Supplementary Notes			
16. Abstract In order to identify the most promising means for improving the flow in the Langley 4- by 7-Meter Tunnel, detailed surveys of the mean velocity profiles were measured in both the horizontal and vertical planes of symmetry at specific locations throughout the tunnel circuit. These data were obtained at test-section dynamic pressures of 1.53, 2.78, and 4.79 kPa (32, 58, and 100 psf, respectively) for tunnel operation in both the closed and open test-section configurations. In the base-line tunnel-flow surveys, the flow patterns near the end of the test section indicate a uniform mean velocity distribution. Downstream of the test section, unsymmetrical flow patterns result in low velocities along the inner walls and in flow separation along the inner wall of the diffuser upstream of the drive fan and along the outer wall of the large diffuser downstream of the drive fan. In order to correct these unsymmetrical flow patterns, a set of trailing-edge flaps attached to the five flow-control vanes located just downstream of the first corner were installed. These flaps were very successful in making the tunnel flow more symmetrical and in eliminating the regions of separation in the diffusers upstream and downstream of the drive fan.			
17. Key Words (Suggested by Author(s)) Velocity profiles Unsymmetrical flow Flow separation Flow deflectors		18. Distribution Statement Unclassified - Unlimited	
		Subject Category 02	
19. Security Classif. (of this report) Unclassified	20. Security Classif. (of this page) Unclassified	21. No. of Pages 53	22. Price A04

For sale by the National Technical Information Service, Springfield, Virginia 22161

NASA-Langley, 1983

National Aeronautics and
Space Administration

Washington, D.C.
20546

Official Business
Penalty for Private Use, \$300

THIRD-CLASS BULK RATE

Postage and Fees Paid
National Aeronautics and
Space Administration
NASA-451



NASA

POSTMASTER: If Undeliverable (Section 158
Postal Manual) Do Not Return
